2019

Dynamics of Competing Structures and Actin Binding Proteins

Christos Langouras
Lehigh University, christos_lagg@hotmail.com

Dynamics of Competing Actin Structures and Actin Binding Proteins

by

Christos Langouras

A Dissertation

Presented to the Graduate and Research Committee

of Lehigh University

in Candidacy for the Degree of

Doctor of Philosophy

in

Physics

Lehigh University

May 2019

Approved and recommended for acceptance as a dissertation in partial fulfillment of the requirements for the degree of Doctor of Philosophy.

Christos Langouras

Dynamics of Competing Actin Structures and Actin Binding Proteins

_____

Defense Date

_____

Prof. Dimitrios Vavylonis
Dissertation Director

_____

Approved Date

Committee Members:

_____

Prof. H. Daniel Ou-Yang

_____

Prof. Ivan Biaggio

_____

Prof. Sabrina Jedlicka

TABLE OF CONTENTS

LIST OF FIGURES

LIST OF TABLES

Abstract

Actin proteins polymerize into many different filamentous structures within individual cells. These actin structures coexist, each playing a significant role in the function of cells. The biophysical basis of this competition however remains an area in need of further investigation. In fission yeast actin patches (nucleated by the Arp2/3 protein complex) and actin cables (polymerized by formin proteins) coexist and regulate endocytosis and cell tip growth, respectively. The available quantitative data and the existence of only two distinct actin structures offer the possibility of using fission yeast as model system to develop quantitative mathematical models to study the interdependence of actin cytoskeleton structures in cells. Recent experimental studies have shown that actin patches and actin cables compete for the same pool of monomeric actin under the regulation of many proteins such as profilin, fimbrin, cofilin, and tropomyosin. To quantify this competition, we developed a mathematical model using a set of differential equations. The model incorporates the most important regulatory factors revealed by prior experiments while using a minimal set of parameter values. In the model actin can be distributed in three pools: patches, cables and cytoplasm. The Arp2/3 complex contributes to patch nucleation and is consumed in patches. Fimbrin and cofilin incorporate in patches and cables and regulate patch and cable lifetime. Profilin binds to actin monomers in the cytoplasm and regulates the elongation rate of actin filaments in cables.

The model captured the main qualitative and quantitative trends in several prior experimental studies, such as the observed increase in ectopic actin filament bundles upon treatment with the drug CK-666 that disassembles actin patches. It can also capture the change in actin patches and actin cables upon underexpression/overexpression of actin, in

combination with CK-666, as well as the increase in actin patch number in cofilin and formin mutants. The model can also describe the change in patch number in experiments of profilin overexpression. The model provides predictions that can be tested in future experiments and illustrates the degree of complexity of mutual dependencies among actin cytoskeletal structures.

The development of actin structures of different structure and morphology depends on many proteins that regulate the dynamics of actin filaments, such as their length, lifetime and binding interactions. In particular, several actin filament side-binding proteins can sever, stabilize or bundle actin filaments. In this study we focused on three of these proteins, namely tropomyosin, cofilin and fimbrin, which are found in many actin cytoskeletal structures. Recent in vitro studies have shown that their actin side-binding dynamics are affected in the presence of each other. In order to study the kinetics and organization of these competing binders along actin filaments, we use stochastic simulations. In the model the actin filament is represented as two independent lattices, representing the two protofilaments of the actin filament double helix. For simplicity, we neglected the mutual dependence between the bound proteins of one protofilament to the other. In accordance with prior in vitro experiments, in our model the binding of a protein to one or more (for the case of tropomyosin) lattice units excludes the binding of proteins of different or same type to these lattice units. Taking into account their actin binding cooperativity properties, we parametrized the model by fitting prior experimental data and using parameters from previous models. The model reveals the range of concentrations where one protein dominates against the other from the start of the simulation until equilibrium but also areas of concentrations where there is a shift of the dominating protein

between early times and equilibrium We find concentration ranges where initially tropomyosin occupies a large portion of the lattice but then either cofilin or fimbrin dominate the equilibrium state. In these cases, we find that while initially cofilin or fimbrin bind in smaller numbers than tropomyosin, they create boundaries that don't allow for long stable tropomyosin chains, so in time tropomyosin is being removed by the lattice. Simulations of actin polymerization that includes tropomyosin, cofilin and fimbrin showed that fimbrin inhibits the elongation of tropomyosin chains on early times, allowing the binding of cofilin on sites where the actin filament hasn't released Pi.

Chapter 1

Introduction to Actin Cytoskeleton in Fission Yeast

1.1 Introduction to Actin Patches and Actin Cables

Actin is one of the most abundant proteins in eukaryotic cells. Actin protein transitions between monomeric and filamentous forms. In cooperation with other proteins that bind to, or nucleate actin filaments, it creates large structures that play an important role in fundamental processes of the cell, such as endocytosis, cell motility and cell division [1-6]. These actin structures exhibit different architectures, such as bundles, dendritic, and contractile structures, which coexist within the same cell. A large number of mathematical and computational modeling based on the biophysical properties of actin filaments, motivated by a larger number of experiments in vitro and cellular systems, has illustrated the plasticity and self-organization properties of the actin cytoskeleton into these various network structures [7-9]. However, how the cell has the ability coordinate the balance among these structures, which use the similar building blocks, as well as remodel them in response to perturbations, remains an important open question for cell biology and biophysics.

Fission yeast, which has three clearly distinct actin cytoskeletal structures, namely actin patches, actin cables, and contractile rings, has been used as a model organism to study the cellular abundance, coordination, and competition among actin structures [10]. The actin patches coexist with actin cables during interphase growth while the contractile ring also forms during mitosis, coexisting with actin patches and actin cables near the ring. These three yeast actin structures have different architectures because their growth is

initiated by distinct actin filament nucleators, namely protein or protein complexes that catalyze the formation of a stable nucleus of actin filament, a process that is otherwise very slow under cellular conditions [4]. Actin patches consist of dense branched short filaments (~ 50nm) nucleated by the Arp2/3 complex, which binds on the sides of actin filaments, nucleating filament branches. During interphase, they assemble and localize mainly at the tips of the cell to promote endocytosis [11, 12]. Actin cables consist of bundled actin filaments and they are several μm in length. The cables are nucleated and polymerized by formin proteins that have the ability to nucleate actin filaments and modify their rate of elongation (i.e. polymerization) by remaining attached as dimers to the polymerizing barbed end of an actin filament. In fission yeast, formin For3 associated to cells tips and elongates cables towards the center of the cell [13, 14]. One of the biological role of actin cables is to serve as tracks for transfer of vesicles towards the growing cell tips [15].

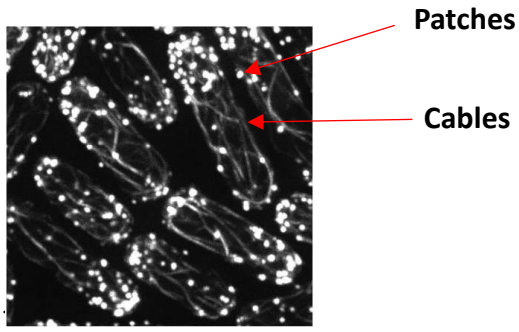

Figure 1.1 Actin patches (bright dots) and actin cables (long lines) in fission yeast cells. Image from [16].

1.1.1 Structure and important Proteins Involved in the Assembly of Actin Patches and Actin Cables

Actin patches are dendritic-like filamentous network structures involving many proteins in their formation. They mediate endocytosis and have a lifetime of ~20 seconds

each [17, 18]. In fluorescence microscopy, patches appear as dots localized mainly in the two tips of the cell (see Figure 1). In a wild type fission yeast cell ~50% of the total actin in the cell is incorporated in patches [19, 20]. Their assembly starts by adaptor proteins binding to clathrin, which is attached in the inner surface of the cell membrane [19, 21, 22]. Proteins that activate the Arp2/3 complex are added to this clathrin-adaptor structure[19, 23]. These proteins enable the Arp2/3 complex to bind to the sides of actin filaments, creating an actin filament side branch, with the help of ATP-actin monomer[24, 25]. Actin monomers from the cytoplasm can bind and start polymerizing at the barbed end of the newly created filament. In this way, this process leads to the creation of branched structures. Capping proteins that bind to the barbed ends block monomer addition and limit branch growth. Cofilin (Adf1 in fission yeast) binds on the sides of actin filaments causing them to break [26, 27]. Fimbrin proteins bind to sides of actin filaments and cross-link them [28]. While the above proteins are believed to be the main regulators of actin patches, many other regulatory proteins are involved [19].

Actin cables consist of actin filaments bundled together with a thickness of ~10 actin filaments in each cable [29]. They help transfer material to the cell tips for cell growth. In a typical cell we estimate ~15% of the total actin to be incorporated in these structures [14, 30]. In fission yeast their formation starts by the formin protein For3 [31]. For3 binds on the cortex of the cell promoting polymerization of actin filaments, which then, are bundled by crosslinking proteins [14]. A crucial factor in their polymerization process is the concentration of profilin protein in the cell. Profilin binds to actin monomers, creating profilin-actin dimers which are estimated to be captured by formins at a ~5 times higher rate than actin monomers [32]. The disassembly of actin cables occurs through the

detachment of For3 from the membrane and cofilin binding on the sides of the actin filaments causing filament severing [31].

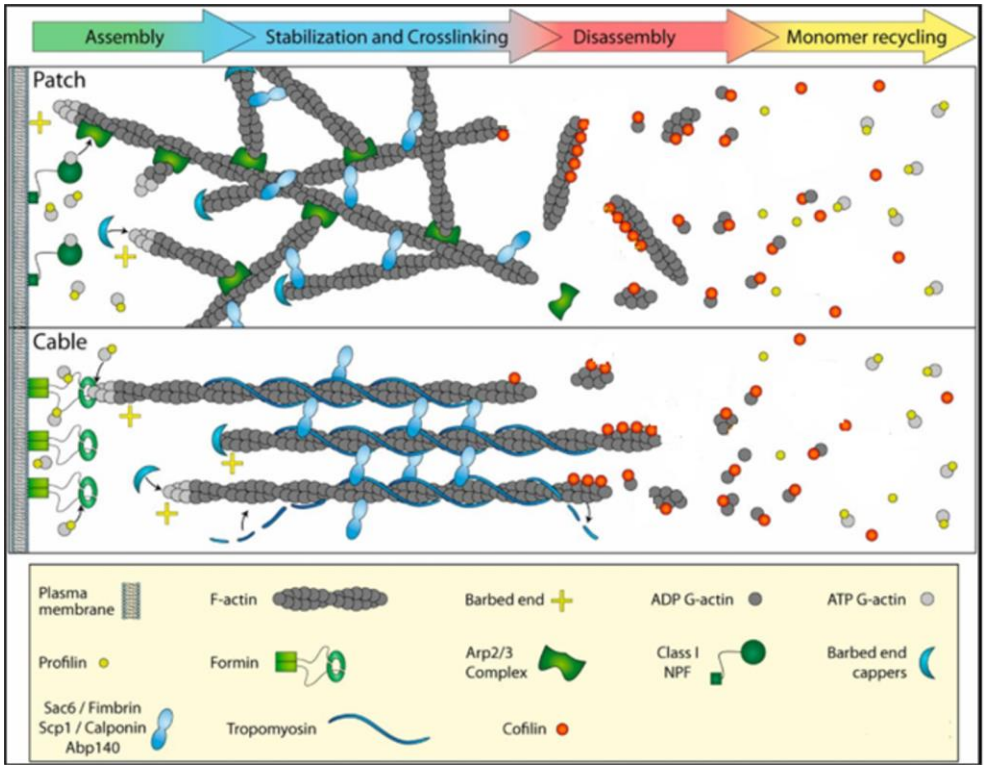

Figure 1.2 Structure of actin patches (top) and actin cables (bottom) and important proteins involved in their formation. Modified image from [33].

1.1.2 Prior Models for Actin Patches and Cables

While there is no theoretical model that account for the competition between actin patches and actin cables, the formation and the dynamics of actin and its regulators in patches and cables have been studied separately. In reference [17], a model at the level of ordinary differential equations was presented for the formation and disassembly of patches, involving many important components of patches. One of the main conclusions in this paper was that severing is the main mechanism for disassembly of actin patches. Figure 1.3 (left panel) shows evolution of patch component numbers versus time when depolymerization is considered to be independent of severing. As shown in the graph, there

is a big difference compared to experiments in the time of accumulation of proteins to actin patches, in particular actin and capping protein disassociate very slowly. Figure 1.3 (right panel) shows that without severing, the value for depolymerization of actin from the ends of the filaments had to be extremely increased in order to match the experimental data. Thus, severing by cofilin, which occurs with higher rate after ATP hydrolysis in the actin filaments, was proposed as the underlying mechanism of patch disassembly. Other studies focus on other aspects of patches like the force patches can exert for membrane invagination [34].

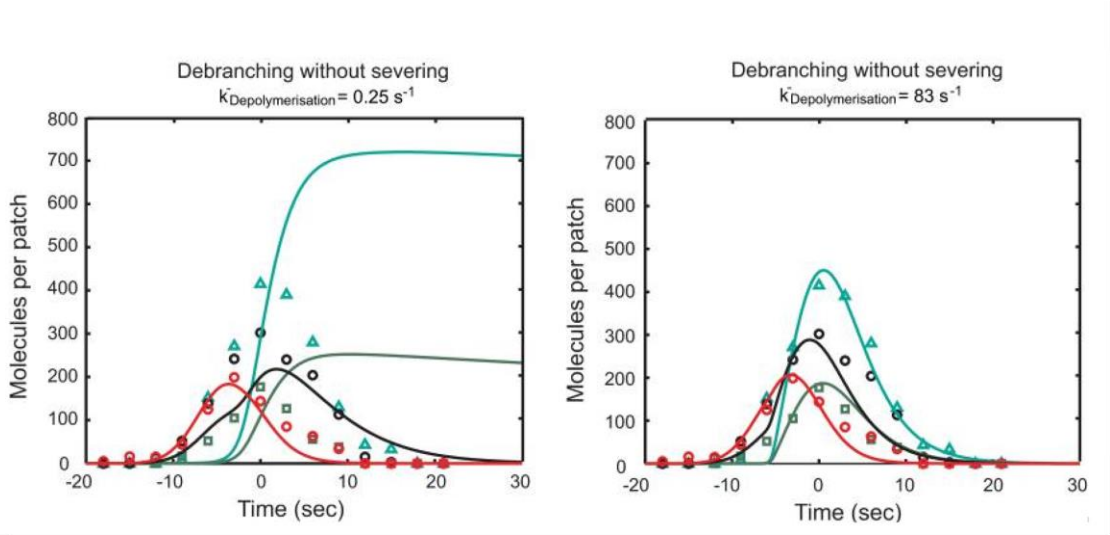

Figure 1.3 Model for actin patch assembly and disassembly from [17]. Graphs show that without severing the model either does not match experiment (left) or else requires a too large rate of actin filament depolymerization (right).

Another study [30] addressed the polymerization-depolymerization cycle of cables with actin filaments formed by formin For3 using a 3D lattice model accounting for diffusion of actin in the cytoplasm and actin cable retrograde flow. In this study the detachment of the formins from the actin cables was assumed to be dependent on the polymerization of actin , based on experiments by [14], which was shown to be important

in regulating actin cables thickness. Other studies used Brownian dynamics simulations to model the spatial organization of actin cables in fission and budding yeast[35].

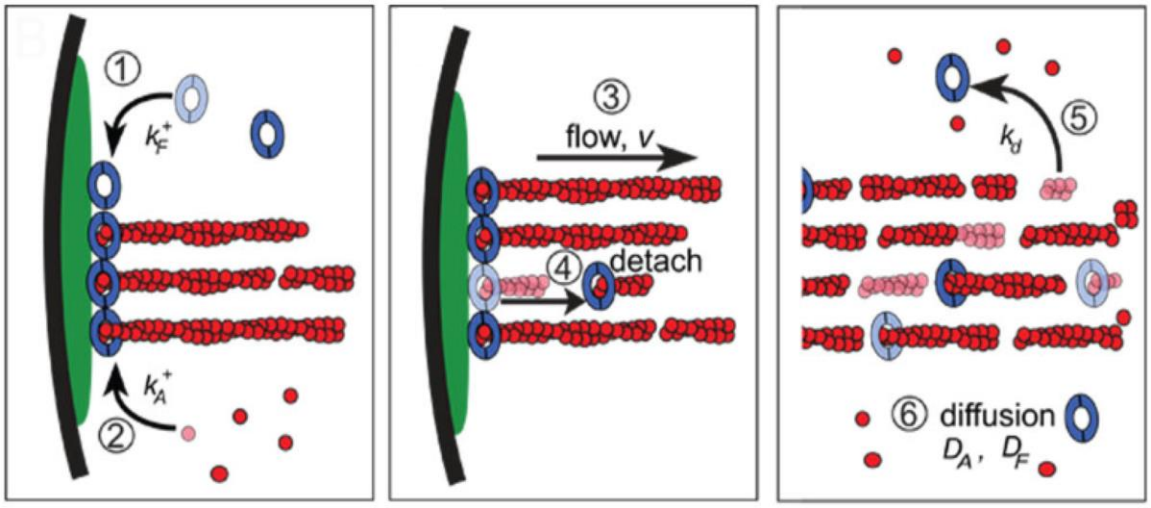

Figure 1.4 Components of the actin cable model in [30].1) Formin For3 (blue) binds on the tip of the cell. 2) Formin recruits actin monomers (red) and accelerates polymerization. 3) Actin filaments undergo retrograde flow by growing from the cell tip towards the center of the cell. 4) Formin detaches from the tip and follows the flow of the actin filaments. 5) For3 and actin disassociates from the cables. 6) For3 and actin diffuse in the cytoplasm from which they can be recycled.

Chapter 2

Model of Competition between Actin Patches and Actin Cables in Fission Yeast

2.1 Motivation and Background

Recent experiments provided data that illustrate the mutual dependence among the three different actin structures in fission yeast. The role of actin concentration and actin filament nucleators was investigated by Burke et al. [36]. These authors showed that inactivation of Arp2/3 complex by drug CK-666 favored the formation of actin -cable-like structures while genetic deletion of formins For3 and/or Cdc12 increased the number of actin patches. When the total actin concentration in the cell was about 5 times higher compared to wild type (WT) cells, this increased the number of actin patches by more than two times (the change in actin cables was harder to detect). Lowering actin concentration by about five times compared to WT decreased the number of actin patches by 66% and lead to a smaller relative decrease of cable-like structures intensity. Interestingly, in the above studies the intensity per actin patch was not significantly modified compared to WT. In the actin over-expression experiments, cells didn't form contractile rings while in the actin underexpression experiments the percentage of cells with rings was doubled.

Other experimental studies further showed the importance of profilin, cofilin and fimbrin in the global regulation of the fission yeast actin system. Suarez et al. [37] showed that changes in the cellular concentration of profilin (which binds monomeric actin and regulates formin-mediated polymerization) influences the number of actin patches, a result which, combined with in vitro data, suggested that profilin favors formin structures as

compared to those constructed by the Arp2/3 complex. Profilin overexpression reduced the fraction of cells with contractile rings and rescued the absence of contractile rings in cells simultaneously overexpressing actin to the WT level [37].

Studies have shown that cofilin is strongly associated with actin cytoskeleton. The presence or absence of cofilin plays a crucial regulatory role in the turnover of the actin cytoskeletal structures [38]. Cofilin has the ability of binding both actin filaments and monomeric actin , and is responsible for severing actin filaments in coordination with other proteins like Aip1. Cofilin localizes both in actin patches and cables and it has been shown to affect the patch lifetime [39].

Fimbrin is another protein that is closely related with actin cytoskeletal structures. Fimbrin crosslinks actin filaments and is associated both with patches and cables. Experiments by Skau et al [18] has shown that deletion of fimbrin in fission yeast cells increased significantly the lifetime of patches and indicated an increase in the accumulation of tropomyosin in patches.

Altogether, these observations support the idea that the different types of actin structures in the cell compete for the same pool of monomeric actin , which is regulated by proteins such as profilin.

The above results imply that understanding the abundance of each actin network in the cell requires consideration of actin dynamics occurring at the whole cell level. These data are demanding of quantitative models that include the most important regulators of the actin system at the whole cell level. Since cellular perturbations influence multiple aspects of the whole actin cytoskeletal system, such quantitative models are important to help interpret the results of experiments, indicate the underlying assumptions, test the

consistency of proposed mechanisms, distinguish direct from indirect effects, support intuitive explanations, and provide insights and testable predictions. Prior modeling studies only considered the dynamics of actin patch and actin cable individually.

While at this point it's not possible to develop a predictive model of the whole actin system at the level of individual molecules (both due to missing experimental data and the early stages of theoretical analysis), here we performed the first step in this direction by developing a mathematical model at the level of mass-action equations. This model considers those major components that have been shown to have an altering effect in the competition between actin structures in fission yeast. The components that we keep track of are actin , Arp2/3 complex, formins, profilin, cofilin, and fimbrin. These can belong to the cytoplasm, actin cables or actin patches (Figure 2.1). We provide equations that describe actin patch and actin cable formation and disassembly, the accumulation of proteins to these two structures, as well as the binding of profilin and cofilin to free actin in the cytoplasm. The system satisfies mass balance and is described by differential equations which account for the partitioning among the different pools (Figure 2.1).

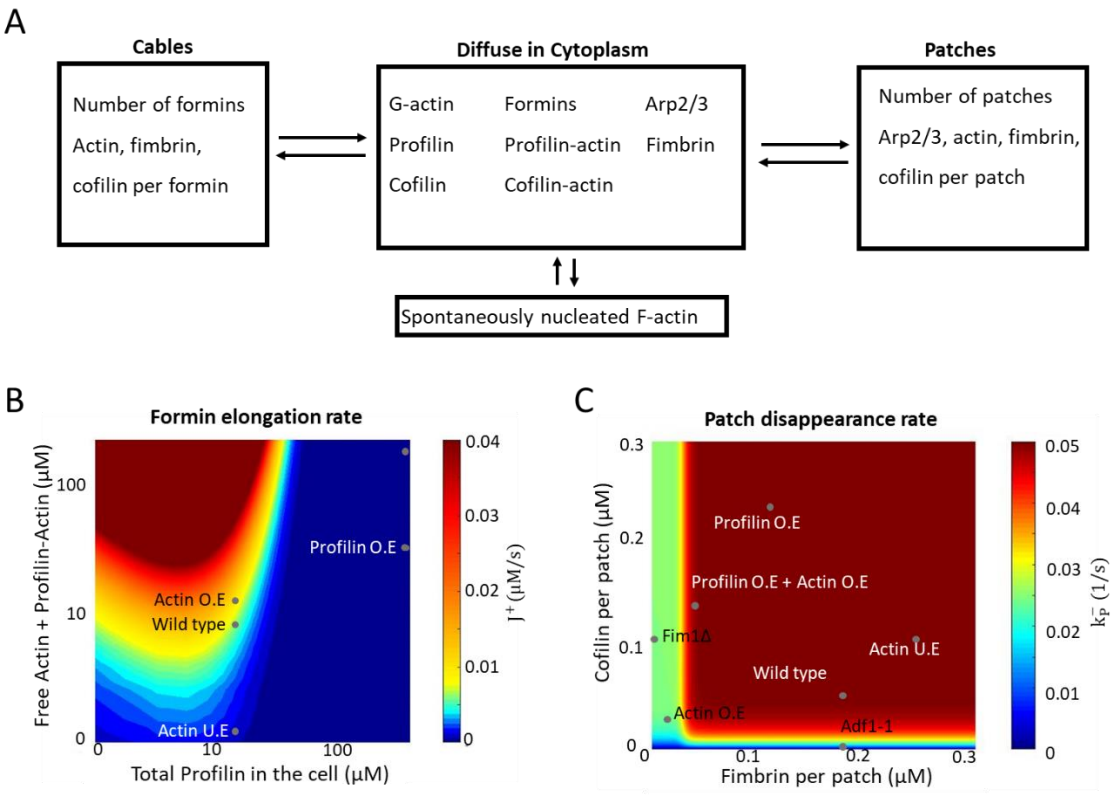

Figure 2.1 (A) Schematic showing the exchange of components between different pools. (B) Assumed elongation rate of filaments formed by formins as a function of the concentration of cytoplasmic actin and total profilin on the system. (C) Assumed disassembly rate of patches as a function of the amount of cofilin and fimbrin per patch. The dots illustrate the predicted steady state of the indicated wild type and mutant cells.

2.2 Mathematical Model and Methods

Actin patches: actin patches are dendritic like filamentous network structures involving many proteins in their formation. While many proteins participate in patches, (many responsible for the activation of the Arp2/3 complex that nucleates actin filament branches), here we attempt a reduced description focused on the important players: actin , Arp2/3 complex, cofilin and fimbrin. In this model we assume that actin patches assembly

is dependent only on the concentration of Arp2/3 complex and the concentration of monomeric actin and profilin-actin complex. In experiments where the total concentration of actin was varied, the actin intensity per patch remained approximately the same, even though the number of actin patches changed [36]. So in our model we consider the number of actin molecules per patch to be constant and just keep track of the number of patches. Further, experiments with overexpression of actin [36] and deletion of fimbrin [18] showed that the lifetime of patches increased and even failed to internalize. We hypothesize that actin patches lacking fimbrin (by deletion or dilution over many patches) were not rigid enough in order to push the endocytic vesicle towards the inside of the cell where they can disassemble, away from the region of Arp2/3 complex nucleation. Based on that, the patch disassembly rate here is considered to have a dependence on the amount of fimbrin per patch. Further experiments have shown that mutation of cofilin has an impact on the lifetime of patches [39] and according to theoretical studies, severing of filaments is needed for disassembly of patches [17]. According to the above assumptions an equation for the number P of actin patches is:

$$\frac{dP(t)}{dt} = (k_P^+ \, G(t) + H((G + Pr_G) - F_P) \, Arp(t) - k_P^- \left(\frac{Fim_P}{P}, \frac{Cof_P}{P}\right) P(t) \, , \qquad (1)$$

where G and Pr_G are free actin and profilin-actin in the cytoplasm, Arp is free Arp2/3 complex in cytoplasm, FimP and CofP is total number of fimbrin and cofilin in actin patches. The functional form of $k_P^- \left(\frac{Fim_P}{P}, \frac{Cof_P}{P}\right)$ is shown in Fig. 2.1C and described below. Parameter F_P is the number of actin per patch and the step function H is introduced such that patches are nucleated only when there is enough actin and profiling-actin in the

cytoplasm. The rate constants in this and following equations were determined by various estimates as described below.

In a typical fission yeast cell there is ~60μM (~10^6 subunits) of actin and ~3μM (~5 10^4subunits) of Arp2/3 complexes so the values for total actin G_{tot} and total Arp2/3 complex Arp_{tot} in the cell are respectively 60μM and 2.5μM [20]. Here and below, the conversion between numbers of molecules per cell and concentrations use the conversion factor of [20] that accounts for the excluded volume of organelles. In fission yeast cell we expect an actin patch to have an amount of 0.42μM (~7000 subunits) of actin and 0.018μM (~300 subunits) of Arp2/3 complexes [19]. In order for ~35% of total actin in the cell to be incorporated into actin patches [20], and considering the amount per patch from [19], we assume that in the steady state of the wild type cell there are 50 patches which falls between ~35 patches reported in [36] and ~70 patches reported in [40].

In the wild type steady state, patches have a lifetime of ~20 seconds [18, 36], thus we assume the disappearance rate of patches in the wild type steady state to be 0.05 s^{-1}. In order to find an expression for the disappearance rate of patches, $k_P^-\left(\frac{Fim_P}{P}, \frac{Cof_P}{P}\right)$, first we use data from [18, 36] showing that when actin is overexpressed by ~5 times or fimbrin is deleted, the lifetime of patches is doubled while actin underexpression by ~5 times doesn't affect patch lifetime. In experiments with temperature sensitive cofilin mutant cells, patches have a much longer lifetime (~30 mins) in the restrictive temperature [39] compared to wild type cells (~20 seconds), indicating that cofilin is necessary for patch internalization. We thus assume the following phenomenological expression that matches the limit of fimbrin deletion and sets the rate to zero in the absence of cofilin:

$k_P^-\left(\frac{Fim_P}{P}, \frac{Cof_P}{P}\right) = \left(1 - \frac{1}{2*\left(1+\left(\frac{Fim_P/P}{0.03}\right)^{10}\right)}\right)\left(1 - e^{-\left(100\ \frac{Cof_P}{P}\right)}\right)$. This expression is plotted in Figure 2.1C.

Actin cables: actin cables consist of actin filaments bundled together with a thickness of ~10 actin filaments per cable [29]. In this study, we considered the amount of actin incorporated in cables and not the actual structure of the cables. Thus, we consider individual actin filaments elongated by active formin For3 at the cell tips, the number of which is dynamic. Every formin elongates a filament with the same rate and this rate has a dependence on the cytoplasmic free actin , profilin-actin and total profilin Pr_{tot} in the cell, $J^+(G, Pr_G, Pr_{tot})$. Regarding the disassembly rate of filaments formed by formins, we assume that it occurs with a rate that depends on the number of cofilin per actin filament, $k_C^-\left(\frac{Cof_C}{C}\right)$, where Cof_C is total cofilin bound to cables and C is number of polymerizing actin filaments in cables. We assumed $k_C^-\left(\frac{Cof_C}{C}\right) = 1 - e^{-\left(100\frac{Cof_C}{C}\right)}$. Here, since the precise dependence of disassembly rate on cofilin concentration in cells is unknown, we assumed it has a similar functional dependence on the disappearance rate of patches, even though these two expressions represent different effects (turnover of whole actin patches that requires internalization versus depolymerization of individual filaments in cables). Denoting F_C the number of actin polymerized by a single formin in cables, the equation describing the incorporation of actin in For3-formed filaments is:

$$\frac{dF_c(t)}{dt} = J^+(G, Pr_G, Pr_{tot}) - k_C^-\left(\frac{Cof_C}{C}\right)F_C(t), \quad (2)$$

where

$$J^{+}(G, Pr_G, Pr_{tot}) = k\left(G(t) + Pr_G(t)\right)\left(e^{-\frac{Pr_{tot}}{1.5\mu M}} + 1\ \mu M^{-1}\ Pr_{tot}\ e^{-\left(\frac{Pr_{tot}}{1.5\mu M}\right)^{0.65}}\right) \quad (3)$$

This phenomenological expression of the elongation of filaments in cables as a function of the concentrations of actin , profilin-actin complex and total profilin in the cytoplasm is showing in Figure 2.1A [41, 42]. By placing the values of the concentrations G, Pr_G and Pr_{tot} we estimated previously in this section in equation (3) a value of the rate constant k = 0.0007 1/s is required to satisfy the steady state. This value gives a polymerization rate of ~100 sub/s at steady state, consistent with [14].

The number of polymerizing For3 formin dimers at cell tips, For_{tip}, obeys

$$\frac{dFor_{tip}(t)}{dt} = k^{+}_{For_{tip}}\ For(t)\ -\ J^{+}(G, Pr_G, Pr_{tot})\left(\frac{For_{tip}}{ptip}\right)\ , \quad (4)$$

where For(t) is formin dimers in cytoplasm and p_{tip}, which represents the average amount of actin processed by the formin before it gets detached from the tip and has a value of 0.12 μM corresponding to 2000 monomers polymerized per formin The rate formins get detached from the tip of the cell and stop polymerizing filaments is proportional to their elongation rate, as described by prior experiments and modeling [14, 30]. By placing the values of the concentrations For_{tip}, $For(t)$, the filament polymerization rate by formins $J^{+}(G, Pr_G, Pr_{tot})$ and processivity p_{tip}, we found a value $k^{+}_{For_{tip}}$= 0.0035 1/s is required to satisfy the steady state.

The estimated amount of incorporated actin in cables is ~15% of total actin in the cell. Assuming that each filament elongated by formin in WT cells is ~4 μm and knowing that an actin monomer is ~2.7 nm [43], we estimate that every formin-formed filament has about 1500 (0.09 μM) actin monomers. To account for 9 μM (~15% of total actin) of actin

in cable filaments, there must be 100 formins elongating filaments at the tips of the cell. Based on the above each actin filament on the cables accumulates 0.09 μM of actin in the WT state.

Active formins in the cytoplasm: Formins can form spontaneous actin filament nuclei and elongate filaments in the cytoplasm [44], an effect that is potentially important under actin overexpression conditions. We assume the number of polymerizing formins in the cytoplasm, $\mathrm{For_{cyt}}$, increase by recruitment of either two free actins or one actin and one profilin-actin with $\mathrm{k^{+}_{For_{cyt}}} = 7\ 10^{-5}\ \frac{1}{\mu M^2\ s}$ [45] :

$$\frac{\mathrm{dFor_{cyt}(t)}}{\mathrm{dt}} = \mathrm{k^{+}_{For_{cyt}}}\ \mathrm{For(t)}\ (\mathrm{G^2(t)} + \mathrm{Pr_G(t)}\ \mathrm{G(t)}) - \mathrm{J^{+}(G, Pr_G, Pr_{tot})}\left(\frac{\mathrm{For_{cyt}}}{\mathrm{pcyt}}\right) \qquad (5)$$

We consider the unbinding of formins from filaments in the cytoplasm to be of the same form as the equation of formin inactivation in the tips of the cell in Equation (4), with parameter p_{cyt} representing the average amount of actin processed by the cytoplasmic formin before it gets detached from the tip. Because the value of p_{cyt} is unknown and there is no evidence suggesting otherwise we choose for p_{cyt} to have the same value as $p_{tip.}$ The equation describing the rate that actin is accumulated by active formins in the cytoplasm is the same as for formins at the tips of the cell, Equation (2).

Spontaneously nucleated filaments: In order to account for the number of spontaneously nucleated filaments we consider the formation of actin nuclei. We consider that actin filaments, with number $\mathrm{N_{sp}}$, can occur with the formation of a nucleus formed by three actin monomers or two actin monomers and a profilin-actin on the barbed end [42, 46]:

$$\frac{dN_{sp}(t)}{dt} = k^{+}_{N_{sp}} * (G^3(t) + Pr_G(t) * G^2(t)) - k^{-}_{cap} * N_{sp}(t) \quad (6)$$

We consider the nucleation rate to be the same for an actin trimer nucleus as for a profilin-actin complex and an actin dimer nucleus too. The rate of nucleation has a value of $k^{+}_{N_{sp}} = 10^{-9}\ \frac{1}{\mu M^2\ s}$ [42] and spontaneously nucleated filaments to cap with a capping rate of $k^{-}_{cap} = 0.2\ 1/s$ [17], a typical value for capping rate in cells [40]. We assume these filaments grow primarily by addition of actin and profilin-actin at their barbed ends with rate constant $k^{+}_{F_{sp}} = 0.006\ \frac{1}{s}$ corresponding to a polymerization rate constant of $10\ \frac{1}{\mu M\ s}$ [47, 48]:

$$\frac{dF_{sp}(t)}{dt} = k^{+}_{F_{sp}} * (G(t) + Pr_G(t)) - k^{-}_{F_{sp}}(\frac{Cof_{Fsp}}{Fsp}) * F_{sp}(t)\ , \quad (7)$$

where F_{sp} is actin per spontaneous nucleated filament. Here, the disappearance rate of these filaments is of the same form as the cofilin-induced disassembly of cable filaments in Equation (2), with Cof_{Fsp} being the cofilin bound to spontaneous nucleated filaments and $k^{-}_{F_{sp}}(x) = k^{-}_{C}(x)$.

Fimbrin: fimbrin proteins bind on the sides of actin filaments and cross-links them [28]. Based on images where fimbrin was tagged with fluorescent protein [19] we assume that most of fimbrin in the wild type steady state is incorporated in patches (Fim_P), while there is also a part of it incorporated in cables (Fim_{For}) and some of it in the cytoplasm (Fim). According to this assumption, we have the following equation for fimbrin incorporated in patches:

$$\frac{dFim_P(t)}{dt} = k^{+}_{Fim_P}\ Fim(t)\ P(t)\ F_{Pfree}(t) - k^{-}_{Fim_P}\ Fim_P(t)\ , \quad (8)$$

where $F_{Pfree}(t)$ is the amount of free binding sites per patch:

$$F_{Pfree}(t) = F_P - (Fim_P(t) + Cof_P(t))/P(t).$$

For fimbrin in formin-formed filaments, Fim_{For} we have:

$$\frac{dFim_{For}(t)}{dt} = k^{+}_{Fim_{For}} Fim(t)\, F_c(t)\, (For_{tip}(t) + For_{cyto}(t))\; F_{Forfree}(t) - k^{-}_{Fim_{For}} Fim_{For}(t), \quad (9)$$

where $F_{Forfree}(t)$ is the amount of free binding sites per filament formed by active formins:

$$F_{Cfree}(t) = F_C - (Fim_{For}(t) + Cof_{For}(t))/(For_{tip}(t) + For_{cyto}(t)) \ .$$

For fimbrin bound to spontaneously nucleated filaments, Fim_{sp}, we have:

$$\frac{dFim_{sp}(t)}{dt} = k^{+}_{Fim_{sp}} Fim(t)\, F_{sp}(t)\, N_{sp}(t)\; F_{spfree}(t) - k^{-}_{Fim_{sp}} Fim_{sp}(t) \quad (10)$$

Where $F_{spfree}(t)$ is the amount of free binding sites per spontaneously nucleated filament:

$$F_{spfree}(t) = F_{sp} - (Fim_{sp}(t) + Cof_{sp}(t))/N_{sp}(t) \quad (11)$$

In order to find the above rate constants of fimbrin association and disassociation with actin patches and actin cables we estimate that in the wild type steady state there is 60% of total fimbrin incorporated in patches, 20% in cables and 20% in the cytoplasm. According to measurements from [20] we expect that in a fission yeast wild type cell there is ~ 5μM (10^5 subunits) of total fimbrin in the cell. These estimations combined with the number of patches are also in good agreement with the estimate that there is ~900 (~0.054μM) of fimbrin per patch in [19]. Fimbrin's association with patches and formin formed filaments

should last less than the lifetime of these structures, so we choose the dissociation rates to be of the order of some seconds: $k^{-}_{Fim_P} = k^{-}_{Fim_{Fp}} = 0.1\ s^{-1}$. By applying the steady state condition, we find the association rate constants $k^{+}_{Fim_P}$ and $k^{+}_{Fim_{For}}$. We assume that the binding rate constant of fimbrin to spontaneously nucleated filaments has the same value as for the formin formed filaments $k^{+}_{Fim_{For}} = k^{+}_{Fim_{sp}}$. By placing the values of the concentrations $Fim(t)$, $F_{Pfree}(t)$, $Fim_P(t)$, the number of patches $P(t)$, and the dissociation rate $k^{-}_{Fim_P}$ we found a value $k^{+}_{Fim_P} = 0.035\ \mu M^{-1}s^{-1}$ is required to satisfy the steady state. Similarly, we find $k^{+}_{Fim_{For}} = 0.02\ \mu M^{-1}s^{-1}$.

Profilin: In this model, profilin has a double role. It binds actin monomers forming actin - profilin complexes which increase the elongation rate of filaments nucleated by formins but also deprives the amount of actin monomers activating Arp2/3 complex [37] through equation (1). The equation describing binding of profilin monomers to actin monomers is:

$$\frac{dPr_G(t)}{dt} = k^{+}_{Pr_G}\ Pr(t)\ \ G(t) - k^{-}_{Pr_G}\ Pr_G(t) \qquad (12)$$

In this work, in accordance with [37] we assume a total of 16 μM of profilin in the cytoplasm of the cell.

Cofilin: Cells expressing fluorescent cofilin had ~200μM concentration in the cytoplasm and ~6000 units per patch. This was under conditions where the cytoplasmic concentration of fluorescent cofilin was ~10 times more than cofilin in WT cells [21]. Therefore, we choose the value of the concentration of the cytoplasmic cofilin in the model to be 20μM. Knowing that cofilin was overexpressed in cofilin fluorescent cells we estimate the number

of cofilin per patch to be less than 6000 cofilin units and we choose the value of 3000 units per patch or 0.18 μM. To our knowledge there are no measurements of the amount of cofilin in actin cables. Thus, we estimate this value according to the ratio of actin in patches and cables and we use the same ratio for active formins in the cytoplasm and spontaneously nucleated filaments. Thus the value of cofilin in the cables is 4.2 μM or 0.042 μM (~700 units) per filament elongated by formin. The incorporation of cofilin in patches, formin formed filaments and spontaneously nucleated filaments is described by the equations below:

$$\frac{dCof_P(t)}{dt} = k^+_{Cof_P}\, Cof(t)\, P(t)\, F_{Pfree}(t) - k^-_{Cof_P}\, Cof_P(t) \quad (13)$$

$$\frac{dCof_{For}(t)}{dt} = k^+_{Cof_{For}}\, Cof(t)\, F_{Cfree}(t)\, (For_{tip}(t) + For_{cyto}(t)) - k^-_{Cof_{For}}\, Cof_{For}(t) \quad (14)$$

$$\frac{dCof_{sp}(t)}{dt} = k^+_{Cof_{sp}}\, Cof(t)\, F_{sp}(t)\, N_{sp}(t)\, F_{spfree}(t) - k^-_{Cof_{sp}}\, Cof_{sp}(t) \quad (15)$$

Cofilin does not bind only on filamentous actin but also monomeric actin [49]. To our knowledge cofilin-actin dimers cannot be incorporated into actin patches or actin cables. Thus there is an amount of monomeric actin reserved from patches and cables. To describe the binding of cofilin to monomeric actin, Cof_G , we use the equation below:

$$\frac{dCof_G(t)}{dt} = k^+_{CofG}\, Cof(t)\, G(t) - k^-_{CofG}\, Cof_G(t) \quad (16)$$

Conservation of mass

As our system is closed, in order to conserve the quantities, we introduce the equations below:

$$G_{tot} = G(t) + F_P\, P(t) + F_C(t)\,(For_{tip}(t) + For_{cyto}(t)) + Pr_G(t) + Cof_G(t) \quad (17)$$

$$Arp_{tot} = Arp_P\, P(t) + Arp(t) \quad (18)$$

$$Fim_{tot} = Fim_P(t) + Fim_{For}(t) + Fim_{sp}(t) + Fim(t) \quad (19)$$

$$Pr_{tot} = Pr(t) + Pr_G(t) \quad (20)$$

$$Cof_{tot} = Cof(t) + Cof_G(t) + Cof_P(t) + Cof_{For}(t) + Cof_{sp}(t) \quad (21)$$

$$For_{tot} = For_{inactive}(t) + For_{cyto}(t) + For_{tip}(t) \quad (22)$$

In order to find the amount of cytoplasmic actin , profilin-actin , cofilin-actin , active cytoplasmic formins, spontaneously nucleated filaments, inactive formins, free profilin and free cofilin in the wild type steady state we solve the system of equations 3,5,6,7,11,15,16,21 and use the known affinities of profilin and cofilin for monomeric actin , K_{dPr}= 0.1 μM and K_{dCofG}= 0.08 μM. [49]. To calculate the steady states of the system for the simulating conditions in Figure 2.2, Figure 2.3, Figure 2.4 and Figure2.5, we wrote a java code implementing Euler's method for the above equations and used a time step of dt = 0.001. In all the runs, the wild type steady state was unique and the same as the long time steady state solution of the differential equations over time.

Component	Value	
P^{WT} (patches in W.T)	50 units	actin patches paragraph

$\mathrm{For_C}$ (formins elongating filaments)	100 units	actin cables paragraph
$\mathrm{Fim_p^{WT}}$ (fimbrin in patches)	3 μM	fimbrin paragraph
$\mathrm{Fim_C^{WT}}$ (fimbrin in cables)	1 μM	fimbrin paragraph
$\mathrm{Fim^{WT}}$ (cytoplasmic fimbrin)	1 μM	fimbrin paragraph
$\mathrm{Fim_{tot}}$ (total fimbrin in W.T)	5 μM	[12]
$\mathrm{Arp_p}$ (arp2/3 per patch)	0.018 μM	[11]
$\mathrm{Arp_{tot}}$ (total arp2/3)	3 μM	[12]
$\mathrm{F_P}$ (actin per patch)	0.42 μM	[11]
$\mathrm{F_C^{WT}}$ (actin on filament in W.T)	0.09 μM	actin cables paragraph
$\mathrm{Pr_{tot}}$ (total Profilin in W.T)	16 μM	[21]
$\mathrm{Pr_G^{WT}}$ (Cofilin bound to monomeric actin)	9.2 μM	profilin paragraph
G_{tot} (total actin in W.T)	60 μM	[12]
$\mathrm{G^{WT}}$(cytoplasmic actin)	0.4 μM	conservation of mass paragraph
$\mathrm{Cof_p^{WT}}$ (cofilin in patches)	4 μM	cofilin paragraph
$\mathrm{Cof_C^{WT}}$ (cofilin in cables)	2 μM	cofilin paragraph
$\mathrm{Cof_G^{WT}}$ (cofilin bound to monomeric actin)	1.2 μM	cofilin paragraph
$\mathrm{Cof^{WT}}$ (cytoplasmic cofilin)	22 μM	cofilin paragraph
$\mathrm{Cof_{tot}}$ (total cofilin)	37 μM	conservation of mass paragraph

2.3 Simulations and Comparison to Experiments

Variation of total actin in the system

In a system like the above it is possible to have multiple steady states and we checked for this possibility. This check was performed for all the cases of Figure 2.3,

Figure 2.4 and Figure 2.5. In order to do this check we used the Matlab numerical solver vpasolve, which can pick random initial conditions from a range of values specified by the user. Over a range of different initial conditions for patches, cables, profilin-actin and cofilin-actin(the rest of the components are dependent) without exceeding the total amount of actin, profilin and cofilin the system creates a volume of ~2.5 10^6 initial conditions. Running vpasolve for 5 10^5 times which gives a resolution of 5 units in the volume of possible initial conditions, we found that the system rests at the same steady state. Knowing that there is only one steady state the next step was to alter the value of total actin and look at the resulting behavior of the system (Figure 2.2). In cases where we decrease the value of total actin by five times (from now on actin U.E.), patches incorporate more actin than cables, while in cases where the total actin is increased by five times (from now on actin O.E.), cables are accumulating most of the actin . The change of abundance of actin in these two structures has to do with the limited number of Arp2/3 complexes in the system. With a certain number of Arp2/3 complexes needed for every patch to get assembled, after some point there is not enough amount of Arp2/3 complex and the production of more patches stops. Thus, in actin O.E condition, cables are left alone without a competitor for monomeric actin and they consume the majority of free cytoplasmic actin.

The change in the abundance of patches in the model is in good qualitatively agreement with the number of patches reported in experiments of the same actin conditions as the ones simulating in this work [36] (Fig. 2.2C). Accumulation of actin in cables on the other hand seems to have a different behavior in simulations and experiments from [36]. The measured fluorescence coming from cables in experiments is about the same in all three actin conditions while in our simulations the amount of actin accumulated in cables

is significantly different. One possible origin of the difference between experimental quantifications and simulations is the lack of bundling of actin filaments in cables. This may occur as a result of lack of enough fimbrin and other crosslinking proteins to connect the filaments elongated by formins into bundles. These proteins may accumulate in the numerous patches and thus actin filaments polymerized by formins may not have a sufficient number of crosslinkers. Thus, they may not have enough intensity to be observed as single filaments by fluorescence microscopy. Indeed, if under actin O.E conditions the accumulated actin in cables is the same as in the WT then this would imply a huge leftover of cytoplasmic actin that cannot be explained by the experimental images in [36]. Another possibility is that the numerous patches under actin overexpression conditions obscure detection of actin cables.

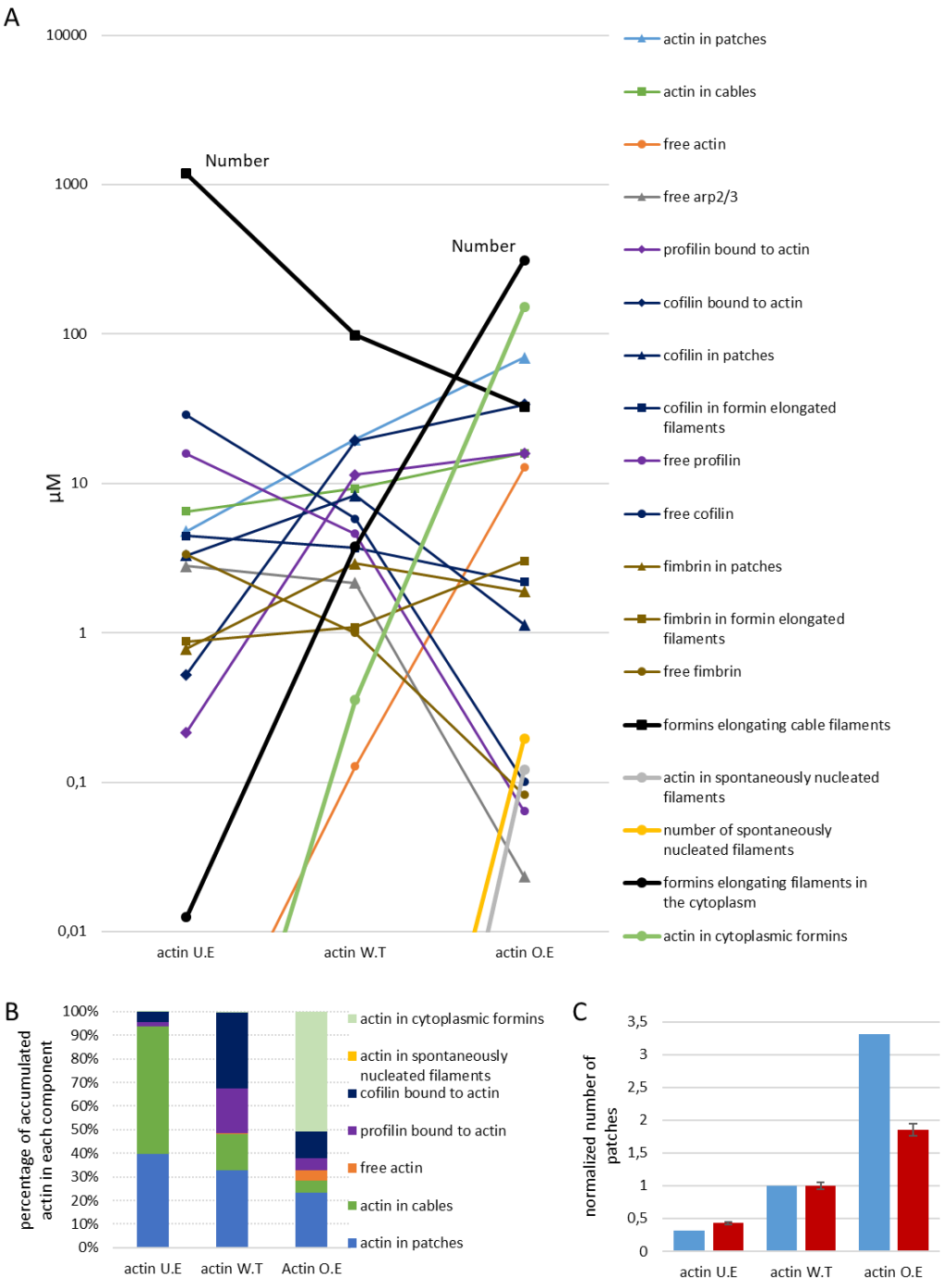

Figure 2.2 A) Values of all the components of the model in steady state in the three actin conditions (actin U.E , actin W.T and actin O.E). In this and following figures, all parameters are in units of µM, except the three indicated curves for formins elongating filaments in cytoplasm, at cell tips and spontaneously nucleated filaments that are shown in absolute numbers (using the same number scale). B) Percentage of the total actin of every component incorporating actin . C) Comparison of normalized number of patches (blue) and experimental data (red) from [36], in the three actin conditions.

Simulating inhibition of Arp2/3 complex

To further study the behavior of this system we set the number of activated Arp2/3 complexes to zero, mimicking the response of WT, O.E and U.E cells to treatment by large doses of drug CK-666 in [36] (Fig. 2.3). This stops the assembly process of patches, leaving cables, formins elongating filaments in the cytoplasm and cytoplasmic filaments as the only structures incorporating actin. In this condition formins take advantage of the absence of patches and we see a growth of the actin accumulated by them. In figure 2.3 A we see that according to different actin conditions the components that benefit the most from the depletion of patches are different. In the actin U.E condition the component that benefits the most is cables as the actin being releasd from patches is not enough to see a rise for filaments from cytoplasmic formins and formins at the tips capture actin faster than profilin and cofilin at these conditions. In actin W.T state while both cables and cytoplasmic formins accumulate actin , cofilin and profilin capture the most. In actin O.E cytoplasmic formins is the only component that benefits from the big amount of actin released from patches. This is happening because there is no reserve of cofilin or profilin to bind on the released actin and cables are in a state where formins at the tips have reached almost an equilibrium in terms of polymerization and detachment. The accumulation of actin by cytoplasmic formins comes doesn’t come from a higher polymerization rate but because there are more cytoplasmic formins elongating filaments.

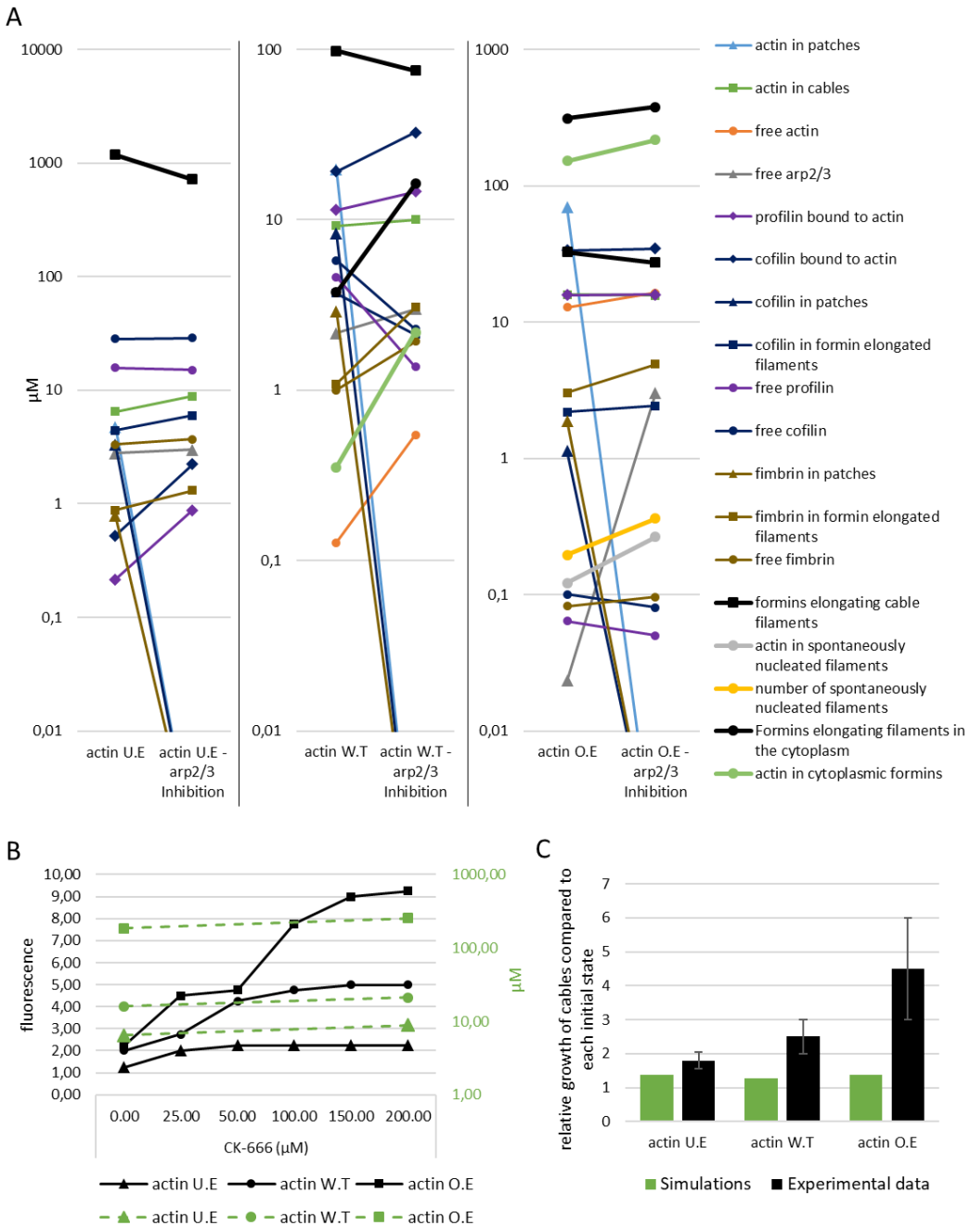

Figure 2.3 A) Values of all the components of the model where inhibition of the activation of Arp2/3 complex is simulated in all three actin conditions. The two black curves for formins elongating filaments in cytoplasm and at cell tips that are shown in absolute numbers. B) Comparison to experimental data (black) from [36], where activation of the Arp2/3 complex was inhibited by different concentrations of CK-666, and data from simulations. Simulations correspond to the highest dose of CK-666 in experiments. C) Increase of actin incorporated in cables after simulating inhibition of Arp2/3 complex for each actin condition (green). Ratio between the final and initial fluorescence state from the experimental data in panel B (black).

Deletion of formin For3

Next, in order to further explore the implications of the competition between patches and cables, we simulated inhibition of the formation of cables by setting the value of formins elongating filaments to zero (Fig. 2.4). This mimics the effect of formin deletion. Assuming all other parameters remain unchanged, we observe a growth in the number of patches by ~ 15% compared to the actin in the WT condition. The low increase in the number of patches aligns with what we would expect as the amount of actin being released from cables is small compared to the amount of actin that patches incorporate before the simulated deletion of formins. For the same reason, we see a low increase of ~10% in the number of patches after removing formins in the actin U.E condition. In actin O.E condition there is a lot of actin being released from cables and we would expect actin from patches to incorporate most of it as cofilin and profilin are not enough to create complexes with much of the monomeric actin . However, the increase of the number of patches is negligible and a large pool of cytoplasmic actin is being created due to the limitation introduced by the available amount of Arp2/3 complex.

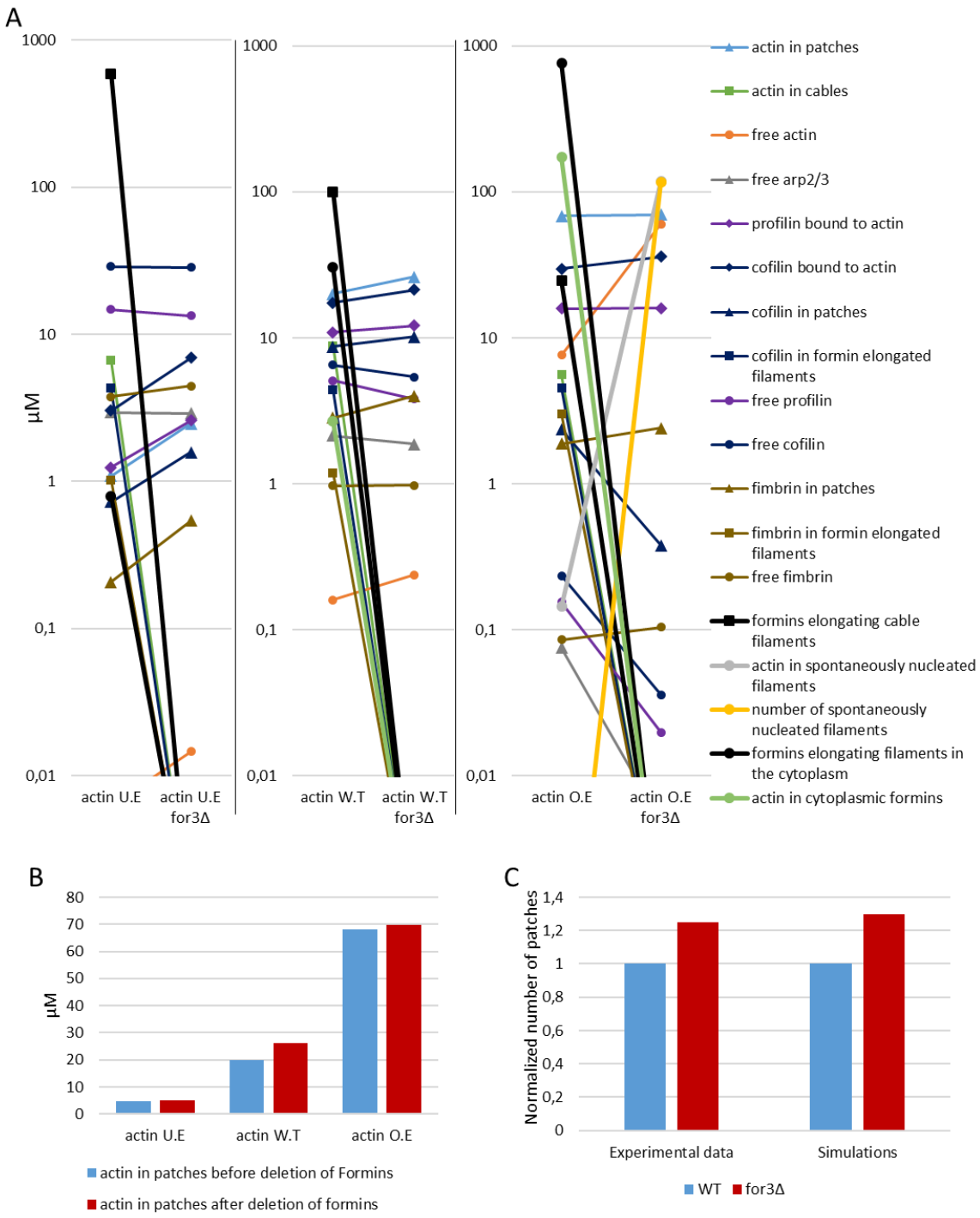

Figure 2.4 A) Values of all the components of the model where deletion of For3 is simulated in all three actin conditions. B) Growth of the number of patches before (blue) and after (red) deletion of For3 formin. C) Comparison between experimental data from ref. [36] and simulations, of growth of patches before (blue) and after (red) deletion of For3 formin, for actin WT condition.

Overexpression of profilin

The concentration of profilin is important for the elongation of cables and thus it is a regulator of the balance between cables and patches. To study the dependence of the system on profilin we increased by ~20 times the initial Pr_{tot} value (Fig. 2.5). The results for the actin incorporated in patches seem to agree with the trend of experimental observations of profilin overexpression from [37]. There are no experimental observations of cables for this particular condition to our knowledge. However, our results are in agreement with the expected behavior of low formin-mediated polymerization rate when the amount of profilin is many times more than the amount of actin (Fig. 2.1B).

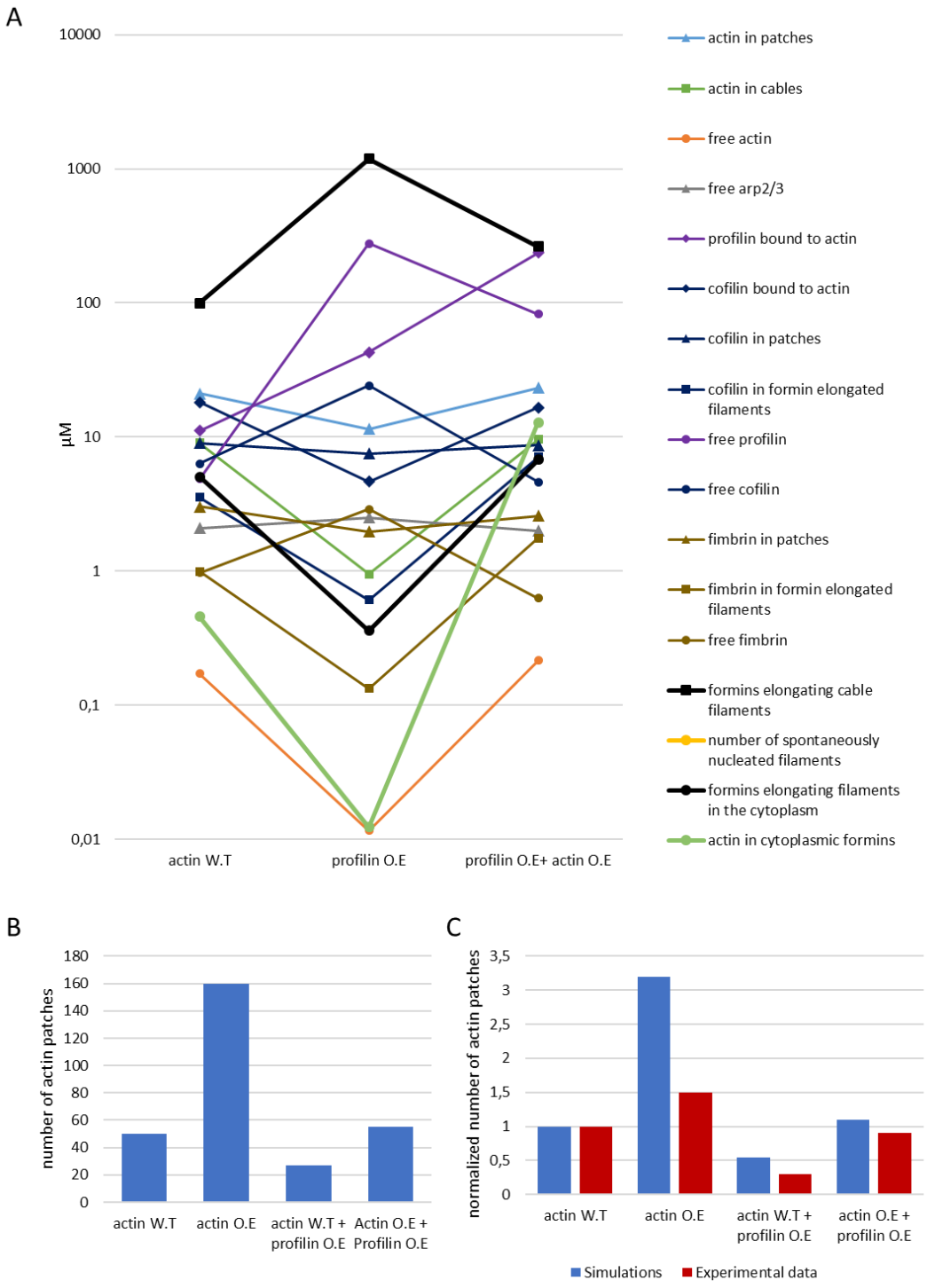

Figure 2.5 A) Graph showing the values of all the components of the model in simulations of overexpression of profilin by 20 times in actin W.T and actin O.E conditions. B) Number of patches for each of the conditions in panel A. C) Comparison of the change in the number of patches between simulations (blue) and experiments (red) from [36] under the same conditions.

Chapter 3

Introduction to Three Actin Filament Side-Binding Proteins

As it was discussed in the previous chapter, actin can polymerize into filaments and many different proteins can bind on the sides of the actin filaments. These proteins have the ability to regulate properties of actin filaments such as lifetime and length or can attach one filament to another creating bundles. In this study we look at three actin filament side binding proteins (tropomyosin, cofilin and fimbrin) which can be found among many different kinds of cells and their effects are important for the proper function of the cytoskeletal structures in these cells. This is motivated by recent experiments suggesting that competition for actin filament side binding between these three proteins is important for regulation of actin dynamics in cells [50].

3.1 Brief introduction to Tropomyosin, Cofilin and Fimbrin

Tropomyosin is closely related to actin cytoskeletal structures with many isoforms that can be found in both muscle and non-muscle cells. In muscle cells tropomyosin plays an important role in muscle contraction [51]. In non-muscle cells the notion is that tropomyosin stabilizes actin filaments by excluding cofilin, which severs actin filaments[52]. Tropomyosin forms dimers with helical shape [53] and different isoforms can span several actin monomers in terms of length. The typical binding affinity of tropomyosin for actin filaments is very low with K_d of ~ 1000 μM [54]. Although tropomyosin has a low binding affinity for actin filaments it can bind in a cooperative manner which increases the binding affinity by 100 to 1000 times depending on the isoform

and salt condition [54, 55]. Thus, cooperativity allows tropomyosin to cover large areas of actin filaments very fast once a stable nucleus of tropomyosin has formed.

Cofilin is another protein that is closely associated with actin cytoskeletal structures and belongs to a family of actin binding proteins which are known to sever actin filaments [56].

Cofilin has the ability of binding both actin monomers and actin filaments but with a higher affinity for actin filaments. Cofilin has an affinity of ~ 10 μM for actin filaments and can bind cooperatively on the actin filament sides [57]. When cofilin binds on the side of an actin filament it accelerates the release of phosphate for several actin monomers away from the binding site [49] and in this way cofilin enhances the turnover of the actin filament from ADP-Pi to ADP states [56].

Fimbrin belongs to the family of actin bundling proteins which are conserved among different cells and cytoskeletal structures [58]. Fimbrin binds on the sides of actin filaments with an affinity of ~0.65 μM [59] and is important in basic functions of cells like endocytosis where its absence has been shown to affect the lifetime of actin patches [18].

3.2 Prior theoretical and experimental studies

Many experimental and theoretical works have studied the thermodynamics and kinetics of tropomyosin binding to actin filaments. Wegner [54] was able to observe the saturation of actin filaments by tropomyosin at different free concentrations at at various magnesium concentrations. Using the McGhee-Von Hippel equation of nearest-neighbor cooperative binding [60], tropomyosin binds loosely on isolated sites but it has high cooperativity (Figure 3.1).

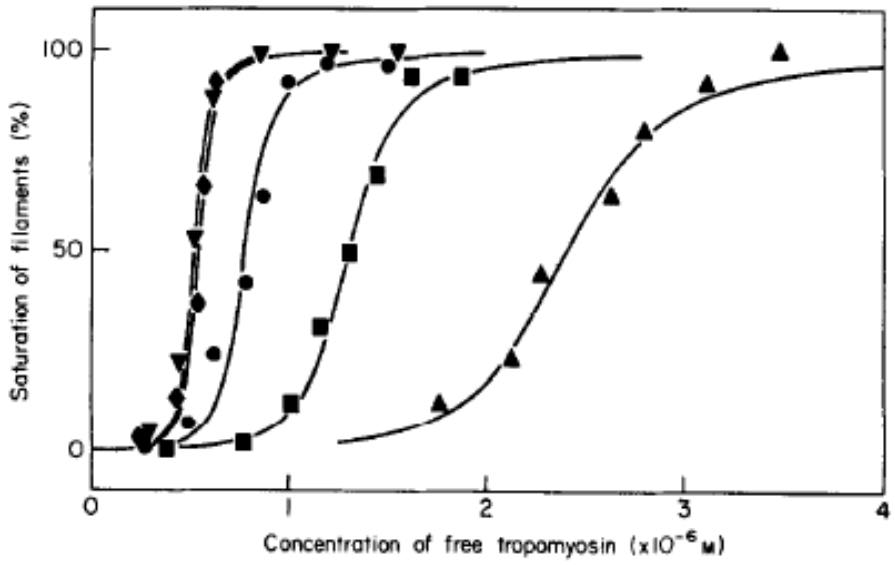

Figure 3.1 Graph from ref. [54] showing the saturation of filaments at free tropomyosin concentrations for different concentrations of magnesium (triangle – 0.5 mM; square – 1 mM; circle – 1.5 mM; diamond – 2 mM; inverted triangle – 2.5 mM).

In a more recent experimental study using TIRF microscopy [55], the authors were able to observe tropomyosin nuclei being formed and elongating on actin filaments. According to images like the one below (Figure 3.2), the binding rate constant to an isolated site and the cooperativity value of tropomyosin were estimated.

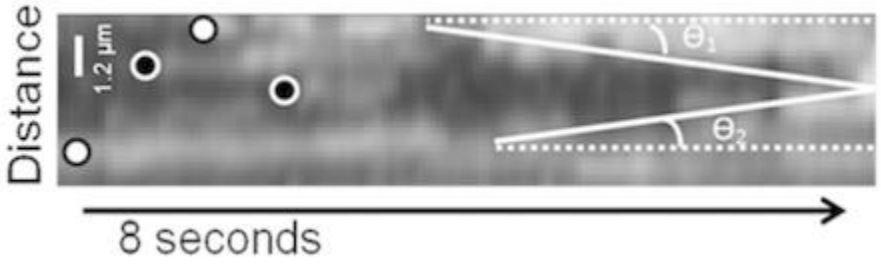

Figure 3.2 Fluorescent tropomyosin binding on actin filament from [55]. White circles represent nuclei of tropomyosin elongating. Black circles represent nuclei of tropomyosin that shrink and disappear.

Experimental studies with human cofilin and skeletal muscle actin [57] revealed the dissociation constant and cooperativity value range by fitting data of occupancy of cofilin in actin filaments against the free concentration of cofilin (Figure 3.3).

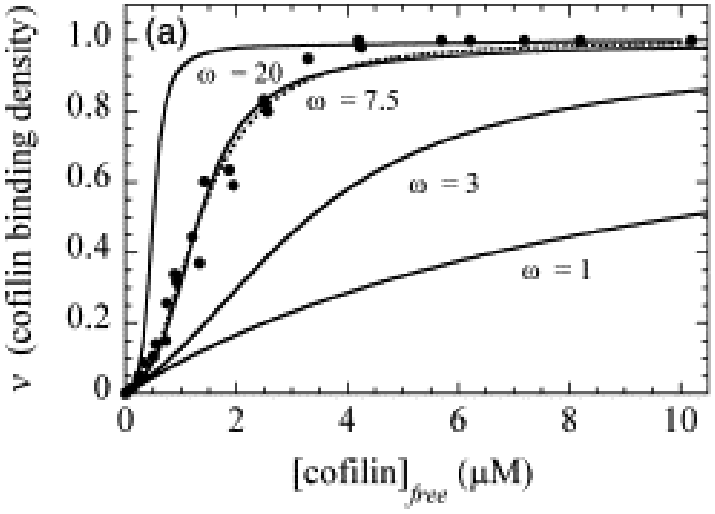

Figure 3.3 Experimental data from equilibrium binding curves in black dots, reproduced from [57]. Black lines represent curves from McGhee-von Hippel equation for fixed single cofilin dissociation constant and different values of cooperativity parameter.

Fitting of a kinetic model to experimental data of cofilin binding to actin in [61] has indicated two states of bound cofilin to actin filaments. In order to match experimental curves of binding and unbinding of cofilin from actin filaments the authors had to introduce to their model an isomerization state according to which bound cofilin could not unbind while being in this state.

By fitting binding and unbind curves to experimental data of fimbrin [18], it was shown that fimbrin doesn't bind cooperatively on actin filaments (Figure 3.4). Thus its binding can be described by the dissociation constant and unbinding rate constant determined from the data in [18].

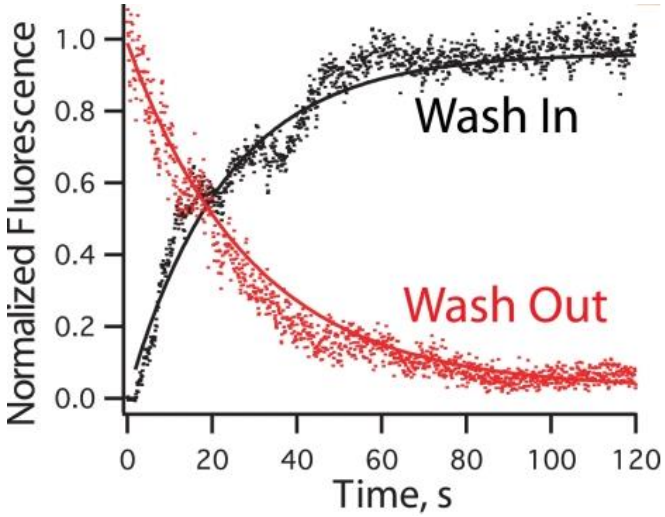

Figure 3.4 Solution of fluorescent fimbrin was washed over single actin filaments (black) and from single filaments (red), from [50].

Recently, an experimental study in vitro [50] revealed aspects of the binding of tropomyosin, cofilin and fimbrin on actin filaments in the presence of each other. For specific concentrations of cofilin and tropomyosin the authors showed that there is competition between tropomyosin and cofilin for actin binding sites as these proteins do not localize on the same parts of the filament (Figure 3.5).

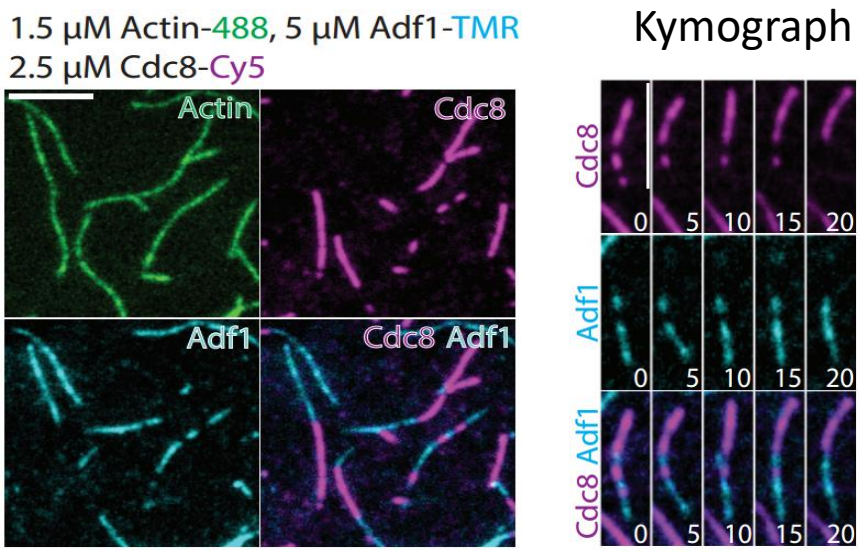

Figure 3.5 *In vitro* experiments with actin (green), tropomyosin (purple) and cofilin (blue). Tropomyosin and cofilin occupy different areas of the actin filaments. In the kymograph we can see that as time passes, tropomyosin is losing the occupied areas at the pointed end of the actin filament (polymerizing at the barbed end) and these areas being overtaken by cofilin.

In these experiments tropomyosin occupied the majority of actin filaments in early times but it was removed by cofilin in later times (Figure 3.5).

From the same study, in experiments where fimbrin was added in the presence of tropomyosin and cofilin, fimbrin inhibited the early binding of tropomyosin to actin filaments (Figure 3.6).

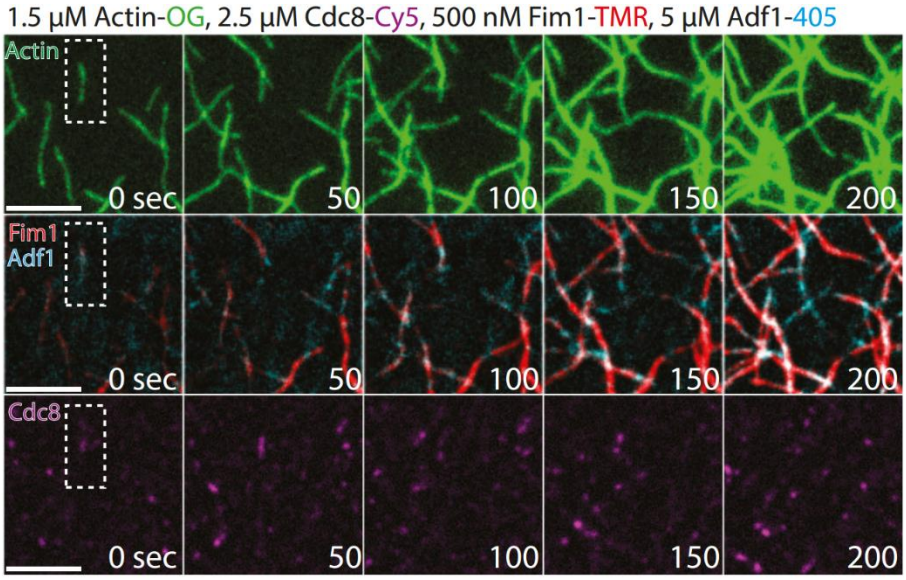

Figure 3.6 *In vitro* experiments with actin (green), tropomyosin (purple), fimbrin (red) and cofilin (blue). As the system is progressing in time, fimbrin occupies the majority of the filamentous actin area. Cofilin is progressing in occupying more area but not as fast as fimbrin. Tropomyosin seems to reach a constant net filamentous area occupancy.

Chapter 4

Methods for Simulating Competitive and Cooperative Binding

While theoretical methods have been developed to predict analytical results for the equilibrium binding of proteins to polymers, the kinetics are much harder to describe with analytical methiods. In order to simulate the competitive binding of different protein species along the actin filament we used the Gillespie algorithm [62]. This method allows to simulate the time evolution of the system using a few number of reactants. In order to make sure that the algorithm I implemented correctly describes the particular system in this study, I compared the data produced by the code to the equilibrium curves produced by analytical methods.

4.1 Comparison of code to McGhee-von Hippel equation equilibrium curves

The McGhee-von Hippel equation [60] can predict the saturation of a one dimensional homogeneous lattice by co-operative or non-co-operative binding of ligands of different lengths according to free equilibrium concentration of the ligand. To test the code against the known McGhee-von Hippel equation, which depends on two parameters (the association constant of single ligand and cooperativity parameter ω), I started by using a simple test ligand having one lattice unit length and no cooperativity (Figure 4.1 A). Then I used a test ligand with one lattice unit length but this time it with nearest-neighbor cooperativity (Figure 4.1 B). Last I tested the code against a ligand which has length of 5 lattice units and also binds cooperatively (Figure 4.1 C). The data points from the simulations match the deterministic curves.

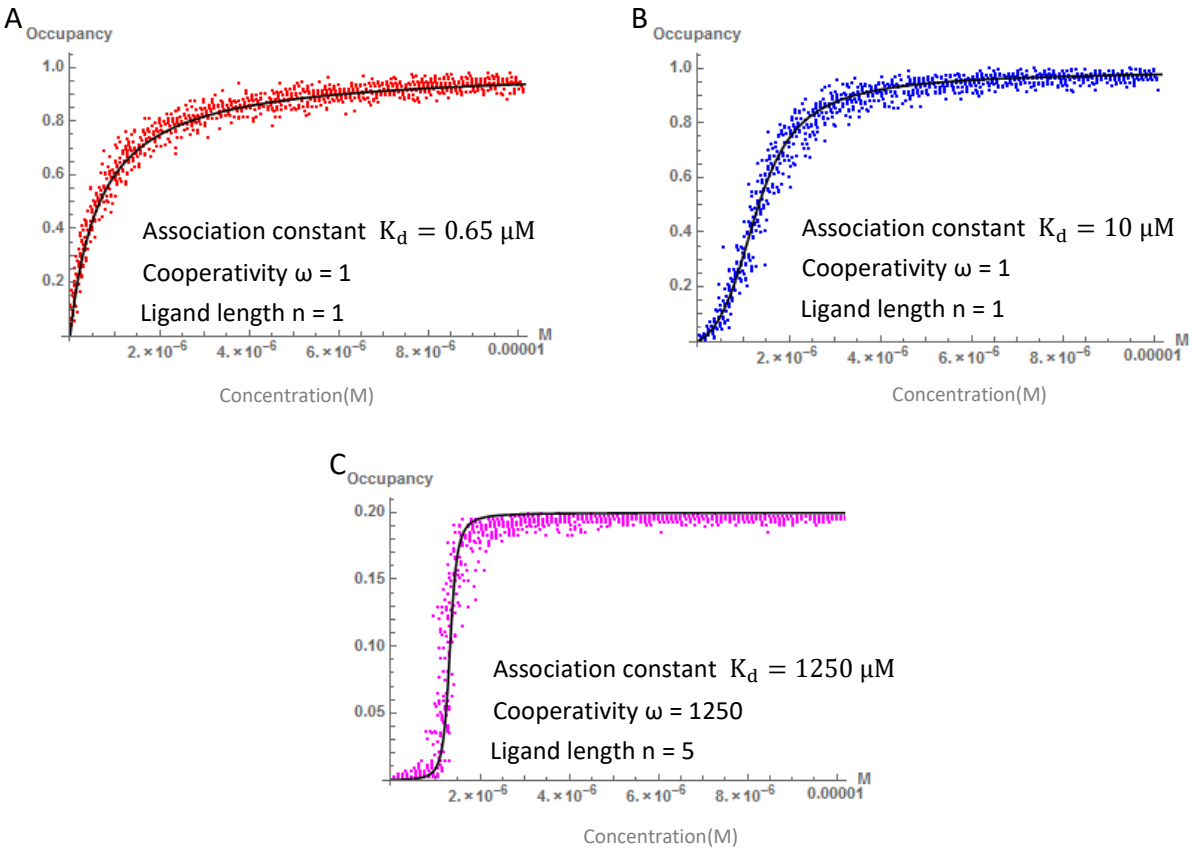

Figure 4.1 A) Ligand with length of one lattice unit without cooperativity. Comparison of simulation (red) to McGhee-von Hippel equation. B) Ligand with one lattice unit length and cooperativity. C) Ligand with a length of 5 lattice units and cooperativity. The noise of simulations originates from the fact that the lattice is not infinite. In all cases the lattice length has been chosen such that it is much longer (100 times) than a single ligand. So in cases A and B the lattice is 100 lattice units long and in C case the lattice is 500 units long.

4.2 Comparison of code to Chen's Method for a pair of test proteins

Chen developed a transfer matrix method [63] that allows to calculate the equilibrium state of different species of ligands bound to a polymer. The ligands can have length more than one lattice unit and also can have cooperative binding. According to this method one expresses the state of the system in the form of a matrix. Calculating the secular equation and derivating with respect to the ligand species free concentration we can find

the equilibrium occupancy of the lattice for this particular species. The drawback of this method, and the reason why I had to use a stochastic method for the simulations, is that the secular equation can be a polynomial of high degree which cannot be solved algebraically [64]. While we were not able to use it to calculate equilibrium occupancy states for the system we want to study (secular equation is a polynomial with greater than 4^{th} order), we used this method to test the validity of the simulations for a pair of test proteins.

I choose the binding affinity for both test proteins to have value $K_a = 2\ \mu M^{-1}$ and the cooperativity value of protein1 $\omega_1 = 2$ and protein2 $\omega_2 = 3$. These cooperativity factors describe the increase in binding affinity next to a neighbor of the same kind as compared to a free lattice. For this test case we assume there is no cooperativity between the two proteins other than the fact that one excludes the other. Both test proteins have a length of 1 lattice unit. For the stochastic simulations we used the Gillespie algorithm [62]. The lattice where the two protein species can occupy is 100 units long, which compared to the one unit size of the test proteins should be enough to give a good correspondence to Chen's method. We let the system run for 5000 seconds for each pair of concentrations and we average over 3 times. The agreement between the stochastic simulations and the analytical method was good (Fig. 4.2)

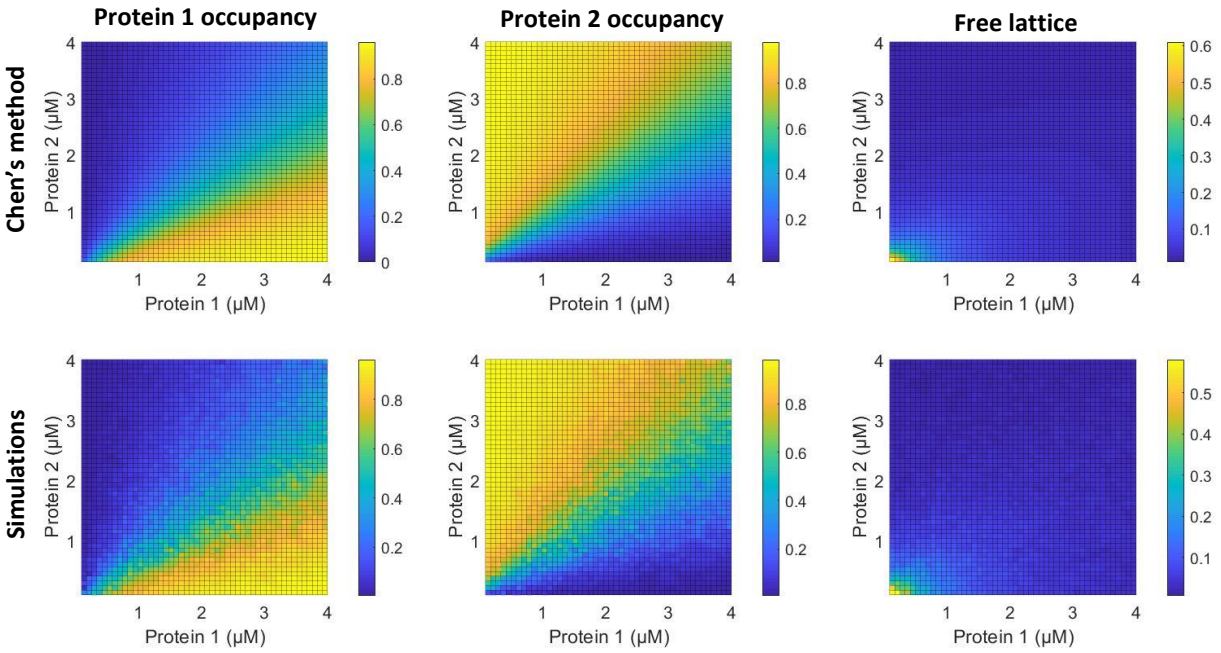

Figure 4.2 Heatmaps showing the lattice occupancy for the two test proteins and the free lattice, using Chen's method [63] and simulations using the Gillespie algorithm method (see main text). The x and y axis refer to free concentrations of Protein 1 and Protein 2.

Chapter 5

Simulations of Competitive Side-Binding to Actin Filaments

5.1.1 Actin filament

The actin filament is composed of two protofilaments in a helical shape. In order to model the binding of the three proteins (tropomyosin, cofilin and fimbrin) on actin filaments, each protofilament is treated as a lattice. Each unit of the lattice represents a binding site of the protofilament and, for simplicity we assume the two lattices are independent of each other (thus we neglect inter-protofilament cooperativity proposed for tropomyosin [50]). Binding to the sides of actin filaments depends on the bound nucleotide composition. To account for the varying nucleotide composition along the filament in simulations with actin filament polymerization, we assume that ATP hydrolysis occurs fast after polymerization and allow each lattice unit to have two states, one with bound ADP-Pi and one bound to ADP. We use a rate of Pi release for bare actin , $k_{Pi\ release} = 0.0019$ 1/s [49, 65]. We assume small Pi concentration in the bulk so once the lattice unit is in the ADP state, it cannot revert back to ADP-Pi-actin .

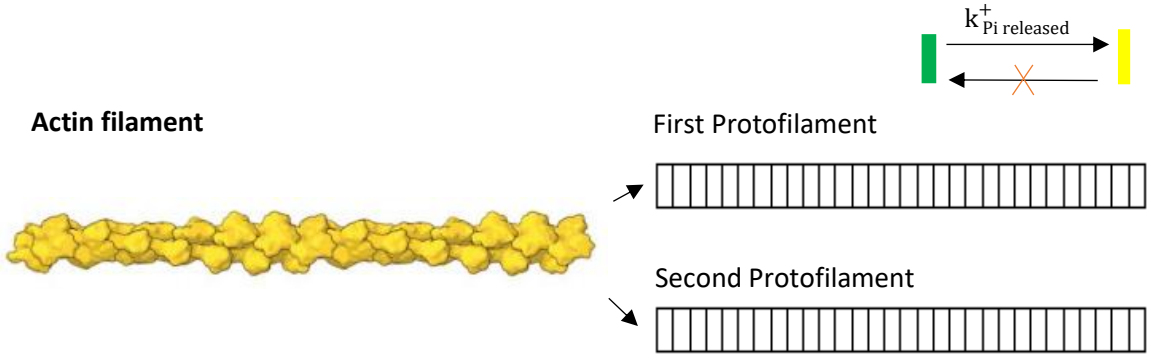

Figure 5.1 Modified image from [66] on the left showing an actin filament. Image on the right shows the implementation of the actin filament in the model. Green color stands for ADP-Pi state and yellow stands for the ADP state.

5.1.2 Tropomyosin

Tropomyosin can extent several monomers, depending on the isoform of tropomyosin. In this model, tropomyosin is assumed to cover 5 lattice units which is consistent with fission yeast tropomyosin that has a length of 4 to 5 actin monomers and we assume that binds in the same way on actin filaments of different nucleotide types (ATP,ADP-Pi,ADP). To calibrate a generic model for tropomyosin, the McGhee-von Hippel model was used in Fig. 5.3 to fit equilibrium binding data of fission yeast tropomyosin to skeletal muscle actin from [50] in order to get values for the binding affinity K_{dtropo} and cooperativity ω values for our reference tropomyosin, shown in Table 5.1. The table also lists our estimates for values for the rate constants of binding and unbinding, combining data from [50, 55]. Knowing the values of Table 5.1, we can solve the equations of the model in Figure 5.2 and find the values of all the parameters needed for modeling the binding of tropomyosin to actin filaments. Here and below we assume the symbols for the equilibrium dissociation constants are equal to the corresponding ratio of dissociation and association rate constants. We assume there is no cooperativity among different proteins other than through excluded volume.

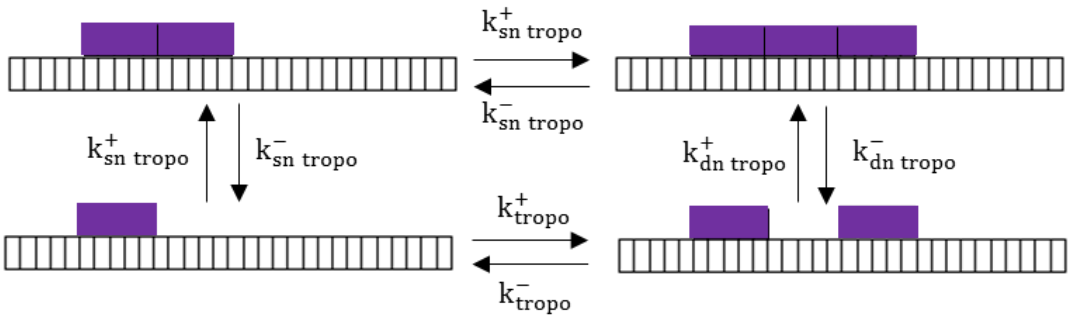

$K_{dtropo} = \frac{k^-_{tropo}}{k^+_{tropo}}$ Dissociation constant for isolated tropomyosin

$\omega = \frac{\omega^+_{sn\ tropo}}{\omega^-_{sn\ tropo}} = \frac{\omega^+_{dn\ tropo}}{\omega^-_{dn\ tropo}}$ Cooperativity

$K_{sn\ tropo} = \frac{K_{dtropo}}{\omega}$ Dissociation constant with one nearest neighbor

$K_{dn\ tropo} = \frac{K_{dtropo}}{\omega^2}$ Dissociation constant with two nearest neighbors

$k^+_{sn\ tropo} = k^+_{tropo}\ \omega^+_{sn\ tropo}$ Binding rate with one neighbor

$k^-_{sn\ tropo} = k^-_{tropo}\ \omega^-_{sn\ tropo}$ Unbinding rate with one neighbor

$k^+_{dn\ tropo} = k^+_{tropo}\ \omega^+_{dn\ tropo}$ Binding rate with two neighbors

$k^-_{dn\ tropo} = k^-_{tropo}\ \omega^-_{dn\ tropo}$ Unbinding rate with two neighbors

Figure 5.2 Schematic of binding and unbinding rate constants of tropomyosin on a protofilament lattice when binding to an isolated site, site with one neighbor and site with two neighbors. Here and below we ensure the rate constants ensure detailed balance is satisfied in equilibrium.

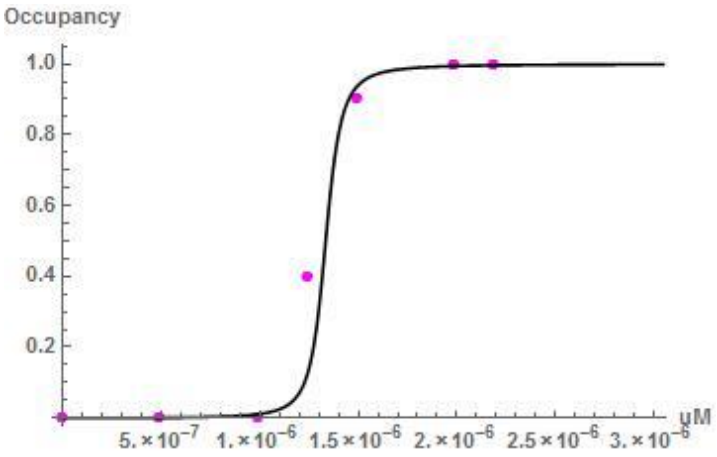

Figure 5.3 Fit of data of cdc8 tropomyosin binding to actin filaments from ref. [50], using the McGhee-Von Hippel model.

Table 5.1 The five parameters that are used to describe the binding and unbinding of tropomyosin to the protofilament lattice. This table shows the independent parameters and the rest of the parameters are found by satisfying detailed balance.

Rate	Value		Source
K_d^{tropo}	1250 μM (fit of experimental data)		Ref. [50] Figure 1B
ω	1000 (fit of experimental data)		Ref. [50] Figure 1B
$k_{sn\,tropo}^{+}$	3	1/(μM s)	Ref. [50] Figure 3D
$k_{dn\,tropo}^{-}$	0.08	1/s	Ref. [50] Figure 4 – Supplement 1
k_{tropo}^{+}	0.1	1/(μM s)	Falls in the range between ref. [55] and the isolated binding rate of cofilin.

5.1.3 Cofilin

Cofilin has size smaller than one actin monomer and in the model we consider cofilin to occupy one protofilament lattice unit. In the model, following previous experimental and theoretical studies, I consider cofilin to bind cooperatively in the lattice [57, 61, 67]. In simulations with varying Pi composition along the filament, we assume cofilin enhanced the release of Pi from the lattice unit it binds, but also the 3 nearest lattice units on the left and right of the bound lattice unit [56] (Figure 5.4 B). The model also accounts for isomerization [61], which is a state where a cofilin molecule cannot unbind. A cofilin molecule can revert back to non-isomerization state and then it can unbind. The parameters needed for the simulation of a "generic" cofilin binding to a lattice were taken from [57, 61, 67] (Table 5.2).

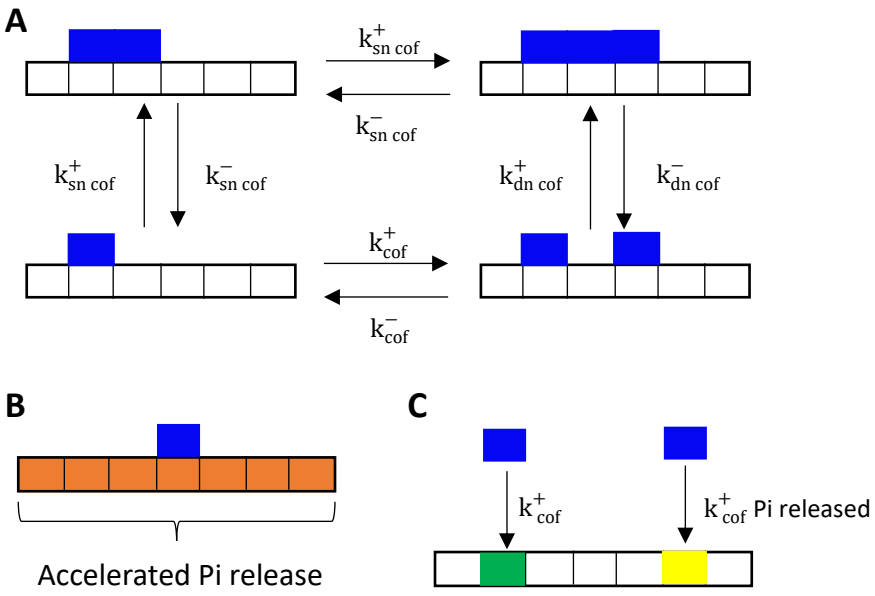

Figure 5.4 A) Binding rate constants of cofilin to the actin protofilament lattice, for an isolated binding site, site with one neighbor and site with two neighbors. B) Binding of cofilin is assumed to accelerate Pi release on the binding site and to 3 lattice units away from it. C) Different binding rate constant of cofilin for the two states of lattice units.

Table 5.2 Parameters that are used to describe the binding and unbinding of cofilin to a lattice. This table shows the independent parameters and the rest of the parameters are found by satisfying detailed balance.

Rate	Value	Source
K_d^{Cof}	10 μM	Ref. [57] Figure 2
ω	7.5	Ref. [57] Figure 2
K_d^{Iso}	1.2 μM	Ref. [61]
k^{+}_{cof} Pi released	0.06 1/(μM s)	Ref. [67] and [61]
k^{-}_{cof}	0.6 1/s	Ref. [67] Table 1
k^{+}_{iso}	0.13 1/(μM s)	Ref. [61]
k^{-}_{iso}	0.16 1/s	Ref. [61]
$k^{+}_{sn\ cof}$	0.16 1/(μM s)	Ref. [67]
$k^{-}_{dn\ cof}$	0.02 1/s	Ref. [50] Figure 6D
k^{+}_{cof}	0.006 1/(μM s)	Ref. [67] Table 1

In in vitro experiments from [50] ~20% of 5 μM of cofilin was labeled with Cy5 and ~1% with TMR. It was estimated that adding 5 μM of cofilin saturated the actin filaments. This 1% of dyed cofilin with TMR allowed for observation of single cofilin unbinding. In order to see if the set of parameters in table 5.2 can match the experimental data we simulated these conditions. In the simulations we keep track of two kinds of cofilin (cofilin1 and cofilin2) to account for the two different dyes in the experiment. As in the simulations the problem of observation of binding and unbinding does not exist we choose 95% to be coflin1 and 5% percent to be cofilin2. The simulation starts and after 100 seconds (to ensure the lattice is occupied by cofilin) the program records the cofilin2 units that bind on the lattice. For each bound cofilin2 there is a timer that stops when the cofilin2 unbinds from the lattice and this time gets recorded. Comparing the recorded data from the simulation to the experimental ones we can see that they are in good agreement(Figure 5.5).

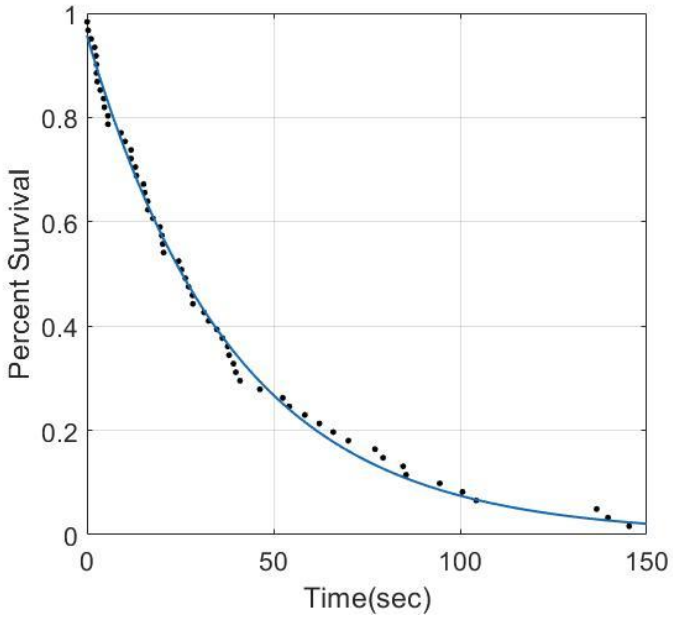

Figure 5.5 Comparison of experimental curve (blue) from [50] where the unbinding times of single cofilin molecules where observed and simulation (black points).

5.1.4 Fimbrin

We assume fimbrin makes contact with one binding site of the actin filament, thus in our model it is considered to occupy one protofilament lattice unit. According to experiments from [59], yeast fimbrin doesn't bind actin filaments cooperatively. Thus, we used only two rate constants to describe the binding behavior of fimbrin to actin filaments. We get these two parameters from the measured dissociation and association rate constants of fimbrin to actin filaments [59].

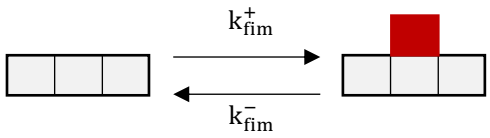

Figure 5.6 Schematic of the binding of fimbrin on the lattice.

Table 5.3 Parameters that are used to describe the binding and unbinding of fimbrin to both ADP- and ADP-Pi-actin lattice.

Rate	Value	Source
K_d^{fim}	0.65 μM	Ref. [59]
k_{fim}^{-}	0.045 1/s	Ref. [59]

5.2 Simulations of competitive binding by tropomyosin, cofilin and fimbrin

5.2.1 Cofilin in the presence of tropomyosin

In order to investigate the dynamics of the competition between tropomyosin and cofilin we performed simulations for a range of concentrations for both tropomyosin and cofilin. Because cofilin binds ATP actin filaments with a much lower single site binding rate than ADP filaments [67], we simulated the binding of tropomyosin and cofilin to both ADP-Pi and ADP-actin lattices, assuming ADP-Pi-actin behaves the same as ATP-actin in

terms of cofilin binding. (Fig. 5.7). In the ADP-Pi-actin lattice (in Fig. 5-7 there is no Pi release), tropomyosin dominates the lattice for concentrations that allow full occupancy by tropomyosin (free tropomyosin larger than 1 μM). Cofilin initially binds very weakly in areas of cofilin high concentrations (8-10 μM) and low tropomyosin concentrations (0.1-3 μM). In equilibrium, the region in the concentration space where cofilin dominates binding to actin is larger compared to the region where it dominates in early times. However in both cases cofilin dominates actin binding in the area of concentration space where tropomyosin is too dilute to saturate the filament. In simulations for binding to ADP-actin, the behavior reverses: cofilin dominates most of the area of concentration space initially and occupies an even larger area in equilibrium. We can observe that tropomyosin is removed from regions of concentration space where it occupied a significant fraction of the lattice initially. Also we can see that even in areas where cofilin occupies only ~50% of the lattice, tropomyosin is still absent. Thus. according to the heatmaps of Fig. 5.6, the state of the filament plays a regulatory role that generally favors tropomyosin for newly polymerized actin and cofilin for aged polymerized actin .

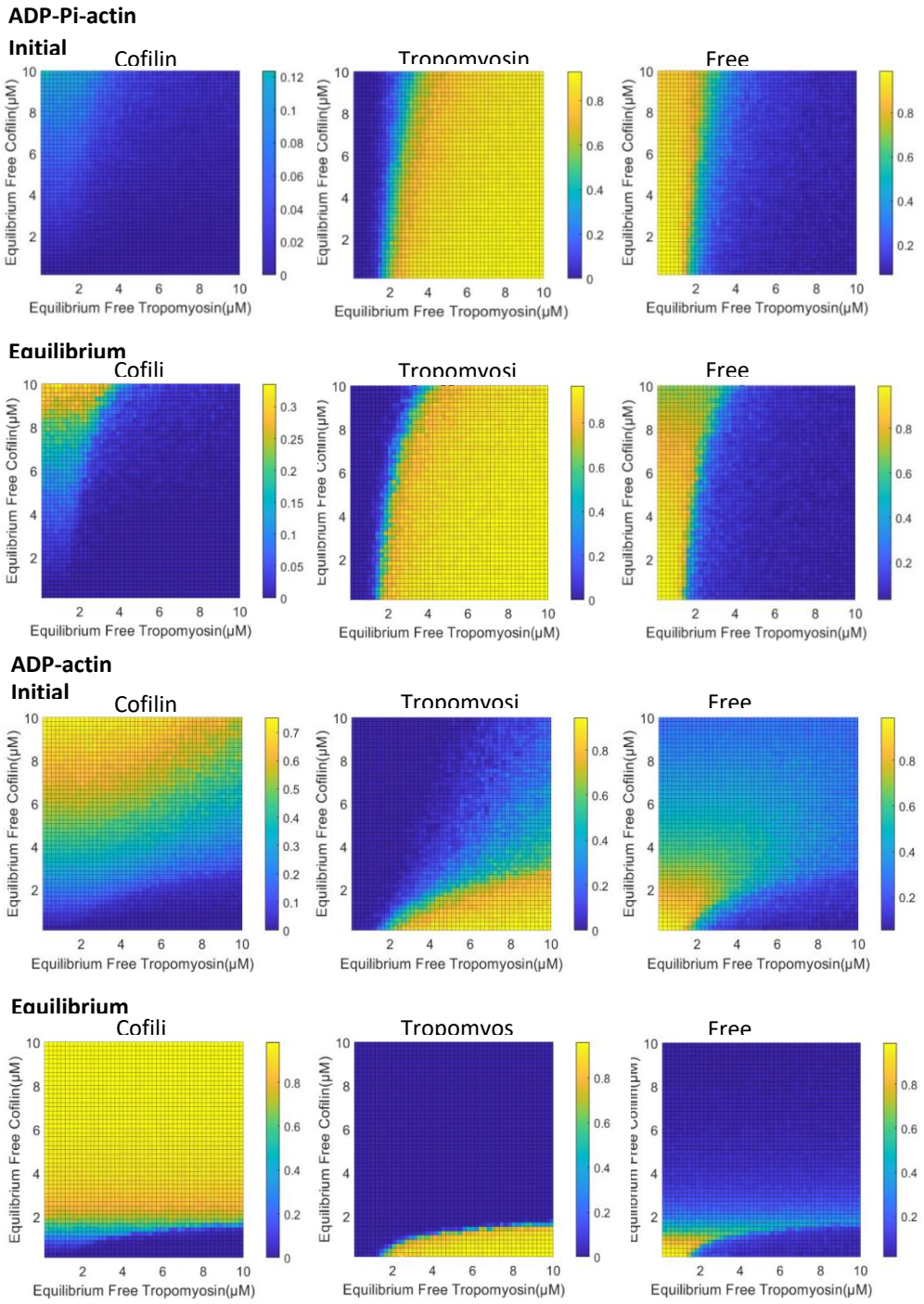

Figure 5.7 Heatmaps of simulated binding of tropomyosin in the presence of cofilin to ADP-Pi- and ADP-actin lattices. Heatmaps after 3 seconds of simulation (initial) in the upper row and 5000 seconds (equilibrium) at bottom. Zero concentrations of cofilin and tropomyosin are not included in the heatmaps. The actin concentration is 1.5 μM. Zero concentrations of tropomyosin and cofilin are not included in the heatmaps.

After observing this shift on the occupancy between ADP and ADP-Pi lattice states between cofilin and tropomyosin, we picked a point of concentrations where this shift occurs (4 μM equilibrium free cofilin, 4 μM equilibrium free tropomyosin). Knowing that these free protein concentrations occur for 7 μM of total cofilin and 4 μM of total tropomyosin in the system when having 1.5 μM of actin, we simulated a polymerizing filament where newly-added subunits are in ADP-Pi state and their state changes state according to random Pi release and cofilin binding enhancement of Pi release. In the simulated kymograph (Fig. 5.7), when the lattice is in the ADP-Pi state, tropomyosin occupies most of the lattice. As time progresses some individual lattice units change to the ADP state but also whole segments where cofilin has bound change to the ADP state. The lattice units that have released Pi allow cofilin to bind more stably on the lattice; due to cooperativity this creates stable nuclei of cofilin which start spreading along the filament. As the cofilin nuclei elongate and spread, they create boundaries along which tropomyosin chains shrink. In this way, as the time progresses, the available lattice space for tropomyosin become less and less and finally tropomyosin is being totally removed from the filament. Another observation is that at long times at which tropomyosin has already been removed, cofilin doesn't fully occupy the lattice: the gaps between individual cofilin and clusters are not long enough for tropomyosin to create a stable nucleus.

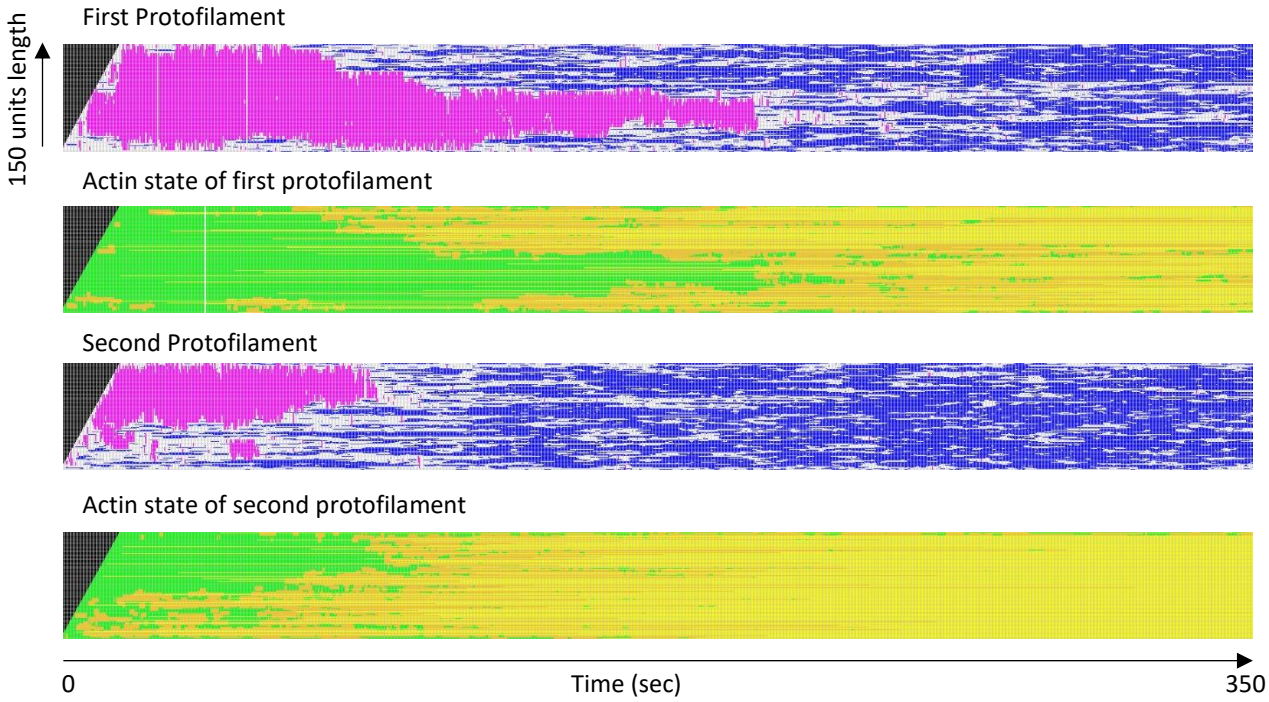

Figure 5.8 Kymograph showing simulation of an elongating filament (two independent lattices) in the presence of initial concentration of 4 μM of tropomyosin and 7 μM of cofilin. The actin concentration is 1.5 μM. The filament starts from 10 units and reaches a total length of 150 units, elongating at 10 units per second. Zero concentrations of fimbrin and cofilin are not included in the heatmaps. Tropomyosin shown in purple, cofilin in blue, free sites in white, ADP-Pi-actin in green, and ADP-actin in yellow.

5.2.2 Competitive binding of cofilin and fimbrin

Cofilin and fimbrin coexist in many cytoskeletal structures, such as yeast actin patches and actin cables discussed in earlier Chapters of this thesis. According to estimates in Chapter 2, the concentration of free fimbrin is ~10 times lower than that of free cofilin in fission yeast cells. Since fimbrin must be able to be present in these structures, we examined the areas of concentration space for which fimbrin dominates over cofilin or the opposite (Fig. 5.8). From the heatmaps in Fig. 5.8 we see that although cofilin can bind

cooperatively on actin filaments, fimbrin has a very low equilibrium dissociation constant, which allows for stable binding over a large region of concentration space.

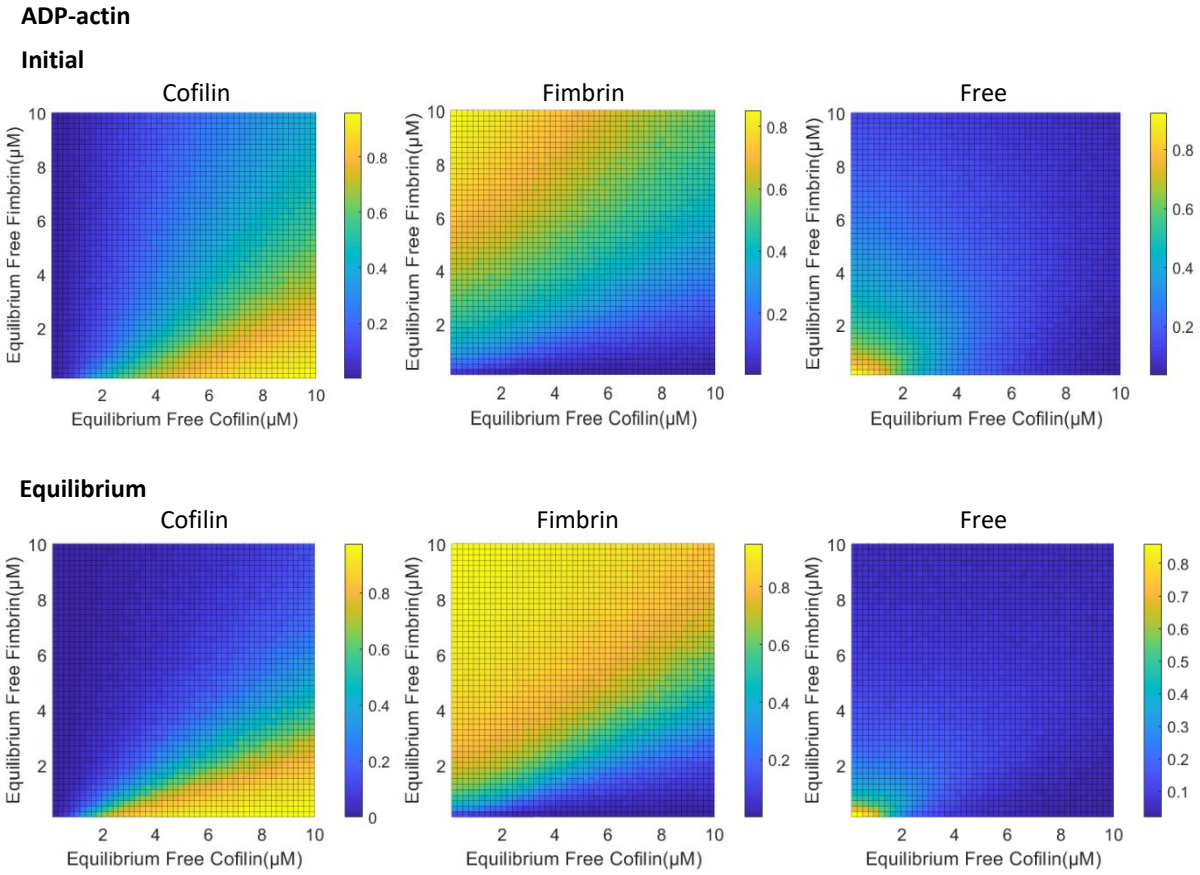

Figure 5.9 Heatmaps of binding of cofilin in the presence of fimbrin to ADP-actin . Heatmaps after 3 seconds (initial) of simulation in the upper row and 5000 seconds (equilibrium) at bottom. The concentrations of free proteins was calculated as in Fig. 5.7. The actin concentration is 1.5 μM. Zero concentrations of fimbrin and cofilin are not included in the heatmaps.

In order to see what would be a possible configuration of fimbrin and cofilin on actin filaments in fission yeast, we simulated the binding of 5 μM of cofilin and 0.5 μM of fimbrin (10 times lower than cofilin concentration) to a lattice that starts from 10 units and reaches at 150 units with an elongation rate of 10 units per second. From the kymograph in Figure 5.9, we can see that at the very early simulation times fimbrin binds sparsely on

the lattice. As the state of the lattice changes to ADP-actin , which allows for tighter binding of cofilin, we see that cofilin covers continuous areas of the lattice that are being interrupted by fimbrin. This configuration has been observed experimentally by [50] and could be of importance in the turnover of actin as cofilin severs filaments in between gaps of cofilin nuclei [68].

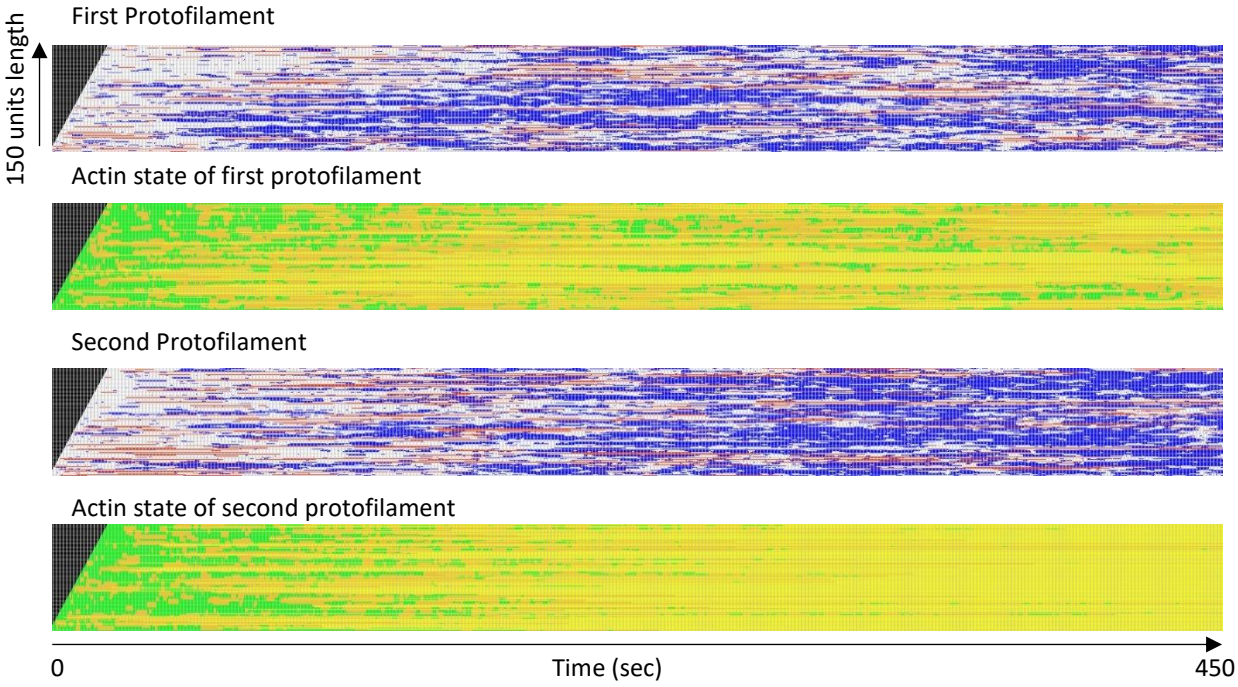

Figure 5.10 Kymograph simulating an elongating filament (two independent lattices) in the presence of initial concentrations of 5 μM of cofilin and 0.5 μM of fimbrin. The lattice starts from 10 units and reaches a total length of 150 units, elongating at 10 subunits per second. The final actin concentration is 1.5 μM. Fimbrin shown in red, cofilin in blue, free sites in white, ADP-Pi-actin in green, and ADP-actin in yellow.

5.2.3 Competitive binding of tropomyosin and fimbrin

Experiments by Skau et al. [18] showed that tropomyosin appears in patches in cells lacking fimbrin, even though tropomyosin cannot be detected in actin patches of wild type

cells. This implied that fimbrin excluded tropomyosin very effectively from actin filaments in patches. Indeed, in heatmaps of fimbrin and tropomyosin competitive binding (Fig. 5.10) we see that fimbrin dominates the lattice initially and continues to do so in equilibrium, for the largest part of the concentration space. Even at areas of concentration where tropomyosin concentration is 10 times higher than that of fimbrin, tropomyosin occupies only a very small fraction of the lattice when fimbrin is present above 1 μM.

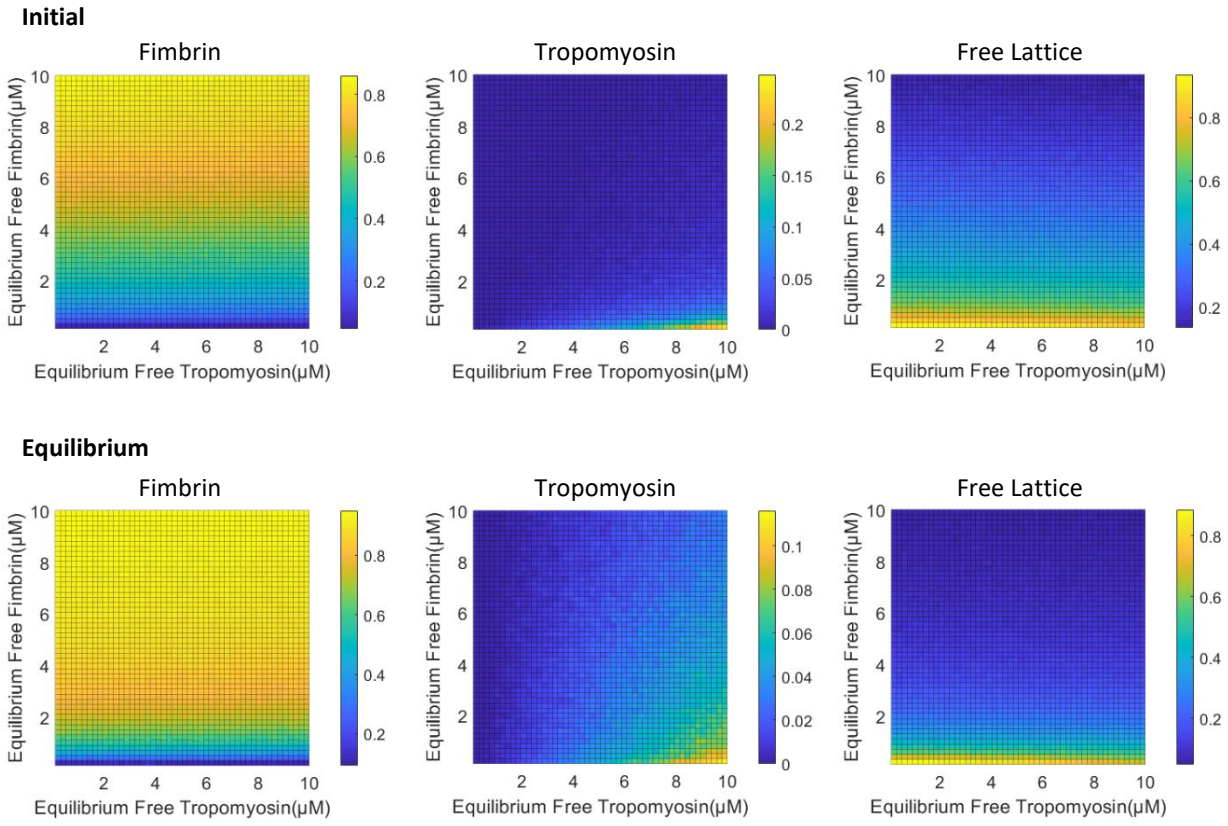

Figure 5.11 Heatmaps of binding of tropomyosin in the presence of fimbrin. Heatmaps after 3 seconds (initial) of simulation in the upper row and 5000 seconds (equilibrium) at bottom. The concentrations of free proteins was calculated as in Fig. 5.7. The actin concentration is 1.5 μM. Zero concentrations of fimbrin and tropomyosin are not included in the heatmaps.

5.2.4 Competitive binding of tropomyosin, fimbrin and cofilin

Knowing that fimbrin generally inhibits the binding of tropomyosin (Fig. 5.11), we tested the suggestion from [50] that fimbrin is working in favor of cofilin, so that cofilin can bind earlier compared to the case when there is only cofilin and tropomyosin present in the simulations. In order to test that, we used the same concentrations as in Fig. 5.8 and 5.10 (where in Fig. 5.8 most of the lattice was occupied by tropomyosin initially). In the kymograph in Figure 5.12 we indeed see that fimbrin binds from early times of the simulation in the lattice and remains there. This creates boundaries for tropomyosin, which is thus unable to elongate from a few stable nuclei. As time progresses, more fimbrin and cofilin bind on the lattice, which together remove tropomyosin about ~10 times faster than cofilin alone in Fig. 5.8.

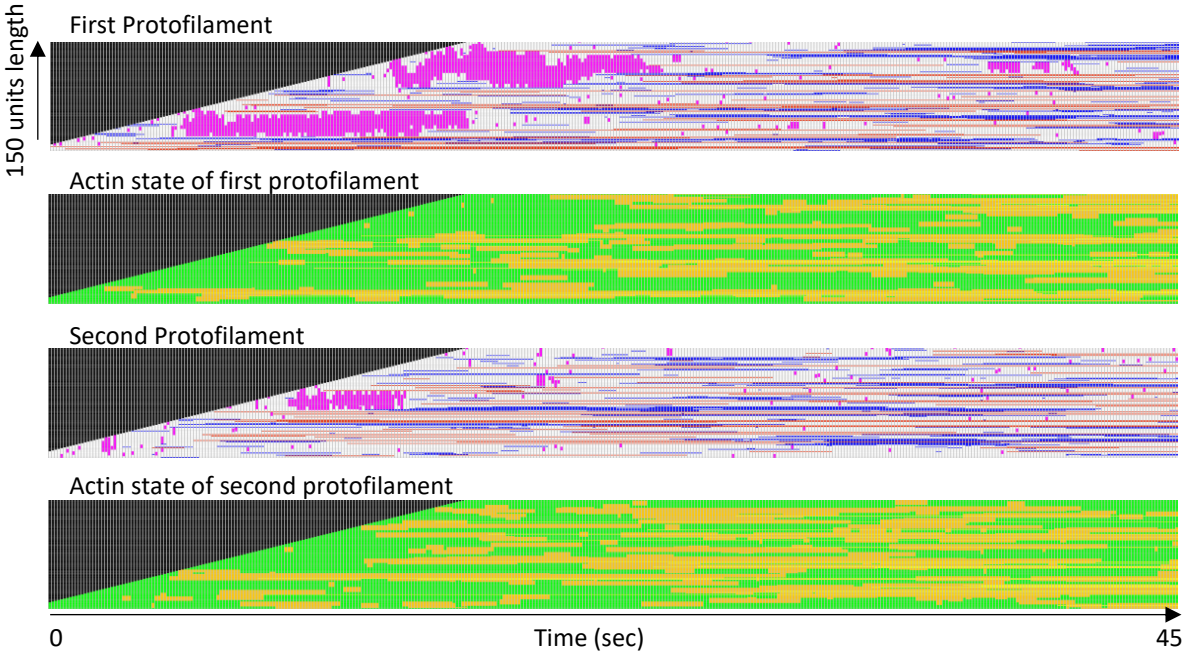

Figure 5.12 Kymograph simulating an elongating filament(two independent lattices) in the presence of 5 μM of cofilin and 0.5 μM of fimbrin. The lattice starts from 10 units and reaches a total length of 150 units, elongating at 10 units per second. The final actin concentration is 1.5 μM. Tropomyosin shown in purple, fimbrin in red, cofilin in blue, free sites in white, ADP-Pi-actin in green, and ADP-actin in yellow.

Chapter 6

Conclusion

In this work I studied the dynamics of actin patches and actin cables in fission yeast and the binding dynamics on actin filaments of proteins that regulate actin cytoskeletal structures. First, in order to study the behavior of actin patches and actin cables when the steady state of the cell is altered, I built a deterministic model of differential equations taking in account the important factors defined by experiments and theoretical models. The model was able to qualitatively match previous experiments from refs. [36, 37] and also explain the mechanisms of the behavior of the system. The model was also able to provide several predictions and show the competition for limited protenin reservoirs for actin patches and cables.

Next, with the aim of studying the binding dynamics of tropomyosin, cofilin and fimbrin on actin filaments, I created a stochastic model accounting for the properties of these three species of actin binding proteins. Simulations of tropomyosin and cofilin showed that there are areas of concentration space where the state of the filament plays an important role in determining which of the two proteins dominates the filament binding sites. Simulations of fimbrin and cofilin showed that cofilin creates continuous bound areas which are separated by few fimbrin molecules. This pattern should promote the severing of filaments by cofilin. Other simulations that included fimbrin and tropomyosin revealed that fimbrin excludes tropomyosin from actin filaments even when the ratio of concentrations is 1 to 10 in favor of tropomyosin. Finally, simulations including tropomyosin, cofilin and fimbrin showed that fimbrin favors the early binding of cofilin by inhibiting the elongation of tropomyosin chains.

Future work in explaining the dynamics of cytoskeletal systems could involve generalizing the model for actin patches and actin cables to other cell types that have similar cytoskeletal structures and actin binding proteins as fission yeast. While further modifications of the model would be needed, such studies could help further elucidate the mechanisms governing the dynamics of cytoskeletal structures. To further study the effect of binding dynamics between tropomyosin, cofilin and fimbrin to actin filaments, a 3D model that accounts for diffusion and severing of filaments could be developed. Such a model could show the different structures of actin filaments created according to the presence of tropomyosin, cofilin and/or fimbrin, and according to the different concentrations of the above three proteins.

Bibliography

1. Pollard, T.D. and J.A. Cooper, *Actin, a central player in cell shape and movement.* Science, 2009. **326**(5957): p. 1208--1212.
2. Balasubramanian, M.K., E. Bi, and M. Glotzer, *Comparative analysis of cytokinesis in budding yeast, fission yeast and animal cells.* Curr Biol, 2004. **14**(18): p. R806-18.
3. Engqvist-Goldstein, A.E. and D.G. Drubin, *Actin assembly and endocytosis: from yeast to mammals.* Annu Rev Cell Dev Biol, 2003. **19**: p. 287-332.
4. Blanchoin, L., R. Boujemaa-Paterski, C. Sykes, and J. Plastino, *Actin dynamics, architecture, and mechanics in cell motility.* Physiological reviews, 2014. **94**(1): p. 235-63.
5. Moseley, J.B. and B.L. Goode, *The yeast actin cytoskeleton: from cellular function to biochemical mechanism.* Microbiol. Mol. Biol. Rev., 2006. **70**: p. 605-645.
6. Pantaloni, D., C.L. Clainche, and M. Carlier, *Mechanism of Actin-Based Motility.* Science, 2001. **292**(5521): p. 1502-1506.
7. Danuser, G., J. Allard, and A. Mogilner, *Mathematical modeling of eukaryotic cell migration: insights beyond experiments.* Annual review of cell and developmental biology, 2013. **29**: p. 501-28.
8. Kim, T., W. Hwang, and R.D. Kamm, *Computational Analysis of a Cross-linked Actin-like Network.* Experimental Mechanics, 2009. **49**(1): p. 91-104.
9. Holz, D. and D. Vavylonis, *Building a dendritic actin filament network branch by branch: models of filament orientation pattern and force generation in lamellipodia.* Biophys Rev, 2018. **10**(6): p. 1577-1585.

10. Kovar, D.R., V. Sirotkin, and M. Lord, *Three's company: the fission yeast actin cytoskeleton.* Trends Cell Biol, 2011. **21**(3): p. 177-87.

11. Kubler, E. and H. Riezman, *Actin and fimbrin are required for the internalization step of endocytosis in yeast.* Embo j, 1993. **12**(7): p. 2855-62.

12. Qualmann, B., M.M. Kessels, and R.B. Kelly, *Molecular links between endocytosis and the actin cytoskeleton.* J Cell Biol, 2000. **150**(5): p. F111-6.

13. Arai, R. and I. Mabuchi, *F-actin ring formation and the role of F-actin cables in the fission yeast Schizosaccharomyces pombe.* J Cell Sci, 2002. **115**(Pt 5): p. 887-98.

14. Martin, S.G. and F. Chang, *Dynamics of the formin for3p in actin cable assembly.* Curr Biol, 2006. **16**(12): p. 1161-70.

15. Pelham, R.J., Jr. and F. Chang, *Role of actin polymerization and actin cables in actin-patch movement in Schizosaccharomyces pombe.* Nat Cell Biol, 2001. **3**(3): p. 235-44.

16. Drake, T. and D. Vavylonis, *Cytoskeletal dynamics in fission yeast: a review of models for polarization and division.* Hfsp j, 2010. **4**(3-4): p. 122-30.

17. Berro, J., V. Sirotkin, and T.D. Pollard, *Mathematical modeling of endocytic actin patch kinetics in fission yeast: disassembly requires release of actin filament fragments.* Mol Biol Cell, 2010. **21**(16): p. 2905-15.

18. Skau, C.T. and D.R. Kovar, *Fimbrin and tropomyosin competition regulates endocytosis and cytokinesis kinetics in fission yeast.* Curr Biol, 2010. **20**(16): p. 1415-22.

19. Sirotkin, V., J. Berro, K. Macmillan, L. Zhao, and T.D. Pollard, *Quantitative analysis of the mechanism of endocytic actin patch assembly and disassembly in fission yeast.* Mol Biol Cell, 2010. **21**(16): p. 2894-904.

20. Wu, J.Q. and T.D. Pollard, *Counting cytokinesis proteins globally and locally in fission yeast.* Science, 2005. **310**(5746): p. 310-4.

21. Chen, Q. and T.D. Pollard, *Actin filament severing by cofilin dismantles actin patches and produces mother filaments for new patches.* Curr Biol, 2013. **23**(13): p. 1154-62.

22. Kaksonen, M., C.P. Toret, and D.G. Drubin, *A modular design for the clathrin- and actin-mediated endocytosis machinery.* Cell, 2005. **123**(2): p. 305-20.

23. Arasada, R., W.A. Sayyad, J. Berro, and T.D. Pollard, *High-speed superresolution imaging of the proteins in fission yeast clathrin-mediated endocytic actin patches.* Mol Biol Cell, 2018. **29**(3): p. 295-303.

24. Sirotkin, V., C.C. Beltzner, J.B. Marchand, and T.D. Pollard, *Interactions of WASp, myosin-I, and verprolin with Arp2/3 complex during actin patch assembly in fission yeast.* J Cell Biol, 2005. **170**(4): p. 637-48.

25. Smith, B.A., S.B. Padrick, L.K. Doolittle, K. Daugherty-Clarke, I.R. Correa, Jr., M.Q. Xu, B.L. Goode, M.K. Rosen, and J. Gelles, *Three-color single molecule imaging shows WASP detachment from Arp2/3 complex triggers actin filament branch formation.* Elife, 2013. **2**: p. e01008.

26. Maciver, S.K., H.G. Zot, and T.D. Pollard, *Characterization of actin filament severing by actophorin from Acanthamoeba castellanii.* J Cell Biol, 1991. **115**(6): p. 1611-20.

27. Carlier, M.F., V. Laurent, J. Santolini, R. Melki, D. Didry, G.X. Xia, Y. Hong, N.H. Chua, and D. Pantaloni, *Actin depolymerizing factor (ADF/cofilin) enhances the rate of filament turnover: implication in actin-based motility.* J Cell Biol, 1997. **136**(6): p. 1307-22.

28. Glenney, J.R., Jr., P. Kaulfus, P. Matsudaira, and K. Weber, *F-actin binding and bundling properties of fimbrin, a major cytoskeletal protein of microvillus core filaments.* J Biol Chem, 1981. **256**(17): p. 9283-8.

29. Kamasaki, T., R. Arai, M. Osumi, and I. Mabuchi, *Directionality of F-actin cables changes during the fission yeast cell cycle.* Nat Cell Biol, 2005. **7**(9): p. 916-7.

30. Wang, H. and D. Vavylonis, *Model of For3p-mediated actin cable assembly in fission yeast.* PLoS One, 2008. **3**(12): p. e4078.

31. Nakano, K., J. Imai, R. Arai, E.A. Toh, Y. Matsui, and I. Mabuchi, *The small GTPase Rho3 and the diaphanous/formin For3 function in polarized cell growth in fission yeast.* J Cell Sci, 2002. **115**(Pt 23): p. 4629-39.

32. Kovar, D.R., E.S. Harris, R. Mahaffy, H.N. Higgs, and T.D. Pollard, *Control of the assembly of ATP- and ADP-actin by formins and profilin.* Cell, 2006. **124**(2): p. 423-35.

33. Goode, B.L., J.A. Eskin, and B. Wendland, *Actin and endocytosis in budding yeast.* Genetics, 2015. **199**(2): p. 315-58.

34. Dmitrieff, S. and F. Nedelec, *Amplification of actin polymerization forces.* J Cell Biol, 2016. **212**(7): p. 763-6.

35. Tang, H., D. Laporte, and D. Vavylonis, *Actin cable distribution and dynamics arising from cross-linking, motor pulling, and filament turnover.* Mol Biol Cell, 2014. **25**(19): p. 3006-16.

36. Burke, T.A., J.R. Christensen, E. Barone, C. Suarez, V. Sirotkin, and D.R. Kovar, *Homeostatic actin cytoskeleton networks are regulated by assembly factor competition for monomers.* Curr Biol, 2014. **24**(5): p. 579-85.

37. Suarez, C., R.T. Carroll, T.A. Burke, J.R. Christensen, A.J. Bestul, J.A. Sees, M.L. James, V. Sirotkin, and D.R. Kovar, *Profilin regulates F-actin network homeostasis by favoring formin over Arp2/3 complex.* Dev Cell, 2015. **32**(1): p. 43-53.

38. Okada, K., H. Ravi, E.M. Smith, and B.L. Goode, *Aip1 and cofilin promote rapid turnover of yeast actin patches and cables: a coordinated mechanism for severing and capping filaments.* Mol Biol Cell, 2006. **17**(7): p. 2855-68.

39. Nakano, K. and I. Mabuchi, *Actin-depolymerizing protein Adf1 is required for formation and maintenance of the contractile ring during cytokinesis in fission yeast.* Mol Biol Cell, 2006. **17**(4): p. 1933-45.

40. Berro, J. and T.D. Pollard, *Local and global analysis of endocytic patch dynamics in fission yeast using a new "temporal superresolution" realignment method.* Mol Biol Cell, 2014. **25**(22): p. 3501-14.

41. Vavylonis, D., D.R. Kovar, B. O'Shaughnessy, and T.D. Pollard, *Model of formin-associated actin filament elongation.* Mol Cell, 2006. **21**(4): p. 455-66.

42. Heisler, D.B., E. Kudryashova, D.O. Grinevich, C. Suarez, J.D. Winkelman, K.G. Birukov, S.R. Kotha, N.L. Parinandi, D. Vavylonis, D.R. Kovar, and D.S. Kudryashov, *ACTIN-DIRECTED TOXIN. ACD toxin-produced actin oligomers*

poison formin-controlled actin polymerization. Science, 2015. **349**(6247): p. 535-9.

43. Howard, J., *Mechanics of Motor Proteins and the Cytoskeleton* 2001, Sunderland, Massachusetts: Sinauer Associates, Inc.

44. Higashida, C., T. Kiuchi, Y. Akiba, H. Mizuno, M. Maruoka, S. Narumiya, K. Mizuno, and N. Watanabe, *F- and G-actin homeostasis regulates mechanosensitive actin nucleation by formins.* Nat Cell Biol, 2013. **15**(4): p. 395-405.

45. Pring, M., M. Evangelista, C. Boone, C. Yang, and S.H. Zigmond, *Mechanism of formin-induced nucleation of actin filaments.* Biochemistry, 2003. **42**(2): p. 486-96.

46. Sept, D. and J.A. McCammon, *Thermodynamics and kinetics of actin filament nucleation.* Biophys J, 2001. **81**(2): p. 667-74.

47. Pollard, T.D. and M.S. Mooseker, *Direct measurement of actin polymerization rate constants by electron microscopy of actin filaments nucleated by isolated microvillus cores.* J Cell Biol, 1981. **88**(3): p. 654-9.

48. Pernier, J., S. Shekhar, A. Jegou, B. Guichard, and M.F. Carlier, *Profilin Interaction with Actin Filament Barbed End Controls Dynamic Instability, Capping, Branching, and Motility.* Dev Cell, 2016. **36**(2): p. 201-14.

49. Blanchoin, L. and T.D. Pollard, *Mechanism of interaction of Acanthamoeba actophorin (ADF/Cofilin) with actin filaments.* J Biol Chem, 1999. **274**(22): p. 15538-46.

50. Christensen, J.R., G.M. Hocky, K.E. Homa, A.N. Morganthaler, S.E. Hitchcock-DeGregori, G.A. Voth, and D.R. Kovar, *Competition between Tropomyosin,*

Fimbrin, and ADF/Cofilin drives their sorting to distinct actin filament networks. Elife, 2017. **6**.

51. Lehman, W., R. Craig, and P. Vibert, *Ca(2+)-induced tropomyosin movement in Limulus thin filaments revealed by three-dimensional reconstruction.* Nature, 1994. **368**(6466): p. 65-7.

52. Ono, S. and K. Ono, *Tropomyosin inhibits ADF/cofilin-dependent actin filament dynamics.* J Cell Biol, 2002. **156**(6): p. 1065-76.

53. Rao, J.N., R. Rivera-Santiago, X.E. Li, W. Lehman, and R. Dominguez, *Structural analysis of smooth muscle tropomyosin alpha and beta isoforms.* J Biol Chem, 2012. **287**(5): p. 3165-74.

54. Wegner, A., *Equilibrium of the actin-tropomyosin interaction.* J Mol Biol, 1979. **131**(4): p. 839-53.

55. Schmidt, W.M., W. Lehman, and J.R. Moore, *Direct observation of tropomyosin binding to actin filaments.* Cytoskeleton (Hoboken), 2015. **72**(6): p. 292-303.

56. Suarez, C., J. Roland, R. Boujemaa-Paterski, H. Kang, B.R. McCullough, A.C. Reymann, C. Guerin, J.L. Martiel, E.M. De la Cruz, and L. Blanchoin, *Cofilin tunes the nucleotide state of actin filaments and severs at bare and decorated segment boundaries.* Curr Biol, 2011. **21**(10): p. 862-8.

57. De La Cruz, E.M., *Cofilin binding to muscle and non-muscle actin filaments: isoform-dependent cooperative interactions.* J Mol Biol, 2005. **346**(2): p. 557-64.

58. Shinomiya, H., *Plastin family of actin-bundling proteins: its functions in leukocytes, neurons, intestines, and cancer.* Int J Cell Biol, 2012. **2012**: p. 213492.

59. Skau, C.T., D.S. Courson, A.J. Bestul, J.D. Winkelman, R.S. Rock, V. Sirotkin, and D.R. Kovar, *Actin filament bundling by fimbrin is important for endocytosis, cytokinesis, and polarization in fission yeast.* J Biol Chem, 2011. **286**(30): p. 26964-77.

60. McGhee, J.D. and P.H. von Hippel, *Theoretical aspects of DNA-protein interactions: co-operative and non-co-operative binding of large ligands to a one-dimensional homogeneous lattice.* J Mol Biol, 1974. **86**(2): p. 469-89.

61. De La Cruz, E.M. and D. Sept, *The kinetics of cooperative cofilin binding reveals two states of the cofilin-actin filament.* Biophys J, 2010. **98**(9): p. 1893-901.

62. Gillespie, D.T., *Exact stochastic simulation of coupled chemical reactions.* The Journal of Physical Chemistry, 1977. **81**(25): p. 2340-2361.

63. Chen, Y.D., *A general secular equation for cooperative binding of n-mer ligands to a one-dimensional lattice.* Biopolymers, 1990. **30**(11-12): p. 1113-21.

64. Chen, Y.D., *Multiple binding of ligands to a linear biopolymer.* Methods Enzymol, 2004. **379**: p. 145-52.

65. Melki, R., S. Fievez, and M.F. Carlier, *Continuous monitoring of Pi release following nucleotide hydrolysis in actin or tubulin assembly using 2-amino-6-mercapto-7-methylpurine ribonucleoside and purine-nucleoside phosphorylase as an enzyme-linked assay.* Biochemistry, 1996. **35**(37): p. 12038-45.

66. Pollard, T.D., *Actin and Actin-Binding Proteins.* Cold Spring Harb Perspect Biol, 2016. **8**(8).

67. Hayakawa, K., S. Sakakibara, M. Sokabe, and H. Tatsumi, *Single-molecule imaging and kinetic analysis of cooperative cofilin-actin filament interactions.* Proc Natl Acad Sci U S A, 2014. **111**(27): p. 9810-5.

68. Andrianantoandro, E. and T.D. Pollard, *Mechanism of actin filament turnover by severing and nucleation at different concentrations of ADF/cofilin.* Mol Cell, 2006. **24**(1): p. 13-23.

CHRISTOS LANGOURAS

Professional Summary

- Modeled systems using Differential Equations, Stochastic Methods, and Statistical Physics
- Operating Systems: Windows, Linux
- Programming Languages: Java, C++
- Software: MatLab, Mathematica, Excel, Kaleidagraph, Origin
- Image Analysis: ImageJ, InkScape
- 3+ years teaching experience: modern and classical physics laboratory, electrodynamics

---

Research Experience

Ph.D Researcher – Lehigh University 2014 - present

- ***Project 1***: Modeled the dynamics of a system of different protein structures that compete for the same resources.
    - Created a system of differential equations
    - Successfully elucidated the mechanisms of these structures by matching existing experiments.
    - The model provided new insights on the behavior of this system of structures that have not been revealed by experiments.
- ***Project 2***: Revealed the dynamics of competition of different protein species for the binding sites of a biopolymer.
    - Used stochastic methods (Monte Carlo).
    - Fitted experimental curves to extract information for parameters.
    - Proven the validity of the model by comparing the experiments to simulations.

- ***Project 3***: Simulated nucleation and elongation of polymers.
    - Used a software developed by my group (TSOAX) to track the appearance and elongation of simulated polymers
    - Analyzed the data from simulations and experimental images produced by TSOAX.

Education

- LEHIGH UNIVERSITY – Doctor of Philosophy in Physics 2014 – 2018
    - Advisor: Prof. Dimitrios Vavylonis
    - Thesis: Dynamics of Competing Actin structures and Actin-Related Proteins in Fission Yeast

- LEHIGH UNIVERSITY – Master of Science, Physics 2013 – 2015

- UNIVERSITY OF IOANNINA – Bachelor of Science, Physics 2007 – 2012
    - Advisor: Prof. Dimitrios Emfietzoglou
    - Thesis: Electron Beam Irradiation Effects on Carbon Nanotubes

---

Awards

- Gerondelis Foundation Graduate Studies Scholarship
2017

- Lehigh University Graduate Student Senate Travel Grant
2016

- Lehigh University College of Arts and Sciences Travel Support
2016

- University of Ioannina Scholarship for Academic Excellence
2008, 2010

Conference Presentations

- PMI annual symposium, Philadelphia, PA 2017
- Qbio Conference, Rutgers University, NJ
  2017
- Biophysical Society Pennsylvania Network Meeting, PennState University, PA
  2017
- American Society of Cell Biology Conference, San Franscisco, CA
  2016
- Biophysical Society Pennsylvania Network Meeting, Lehigh University, PA.
  2016